Connectivity of scamp (*Mycteroperca phenax*) populations in the United States Gulf of Mexico and Atlantic Ocean

Authors: J. Roger Brothers*[1], Kyle W. Shertzer[2], Mandy Karnauskas[3], Ana C. Vaz[3,4], Nathan M. Bacheler[2], Claire B. Paris[4]

*Corresponding author email: jroger.brothers@gmail.com

[1] University of Maine, School of Marine Sciences

350 Commercial Street, Portland, ME 04101, U.S.A.

[2] National Oceanic and Atmospheric Administration, Southeast Fisheries Science Center

101 Pivers Island Road, Beaufort, NC 28516, U.S.A.

[3] National Oceanic and Atmospheric Administration, Southeast Fisheries Science Center

75 Virginia Beach Drive, Miami, FL 33149, U.S.A.

[4] University of Miami, Rosenstiel School of Marine, Atmospheric, and Earth Science

4600 Rickenbacker Causeway, Miami, FL 33149, U.S.A.

ABSTRACT:

Connectivity among marine fish populations not only arises through the movement of adults, but also through larval dispersal facilitated by ocean currents. For species with long pelagic larval duration and high site fidelity as adults, larval dispersal can be the dominant mechanism of connectivity among otherwise spatially distinct populations. Therefore, when assessing the recruitment dynamics or population structure of such species it is essential to evaluate how larval biology and reproductive ecology interact with oceanographic circulation. To investigate this for scamp (*Mycteroperca phenax*), a grouper found in the Gulf of Mexico and Atlantic Ocean, we simulated the dispersal of millions of virtual larvae throughout scamp's range near the southeastern United States. We found a pattern of local retention, with larvae tending to settle close to their spawning location. There was also, however, long-distance dispersal that consistently crossed the boundary between spatial management units. Due to directional patterns in oceanographic transport, and spatial differences in abundance, almost one-third of the virtual larvae that settled in the Atlantic came from spawning locations in the Gulf of Mexico, although most of these settled near the boundary between the regions. These patterns were robust to a variety of sensitivity analyses, but the magnitude of connectivity between management units varied. This connectivity has significant implications for stock assessment and fishery management. It may increase the resilience of Atlantic populations, but it also means the sustainability of Atlantic populations may rely, in part, on the health of spawning populations in the Gulf of Mexico.

KEYWORDS: connectivity, larval dispersal, grouper, reef fish, stock structure, fisheries management

1. INTRODUCTION

Movement patterns and site fidelity strongly influence the population connectivity and spatial structure of genetic differentiation in a species. Connectivity requires movement, so species with high movement rates or distances are commonly associated with a high degree of mixing and more homogeneous genetic structure on broad spatial scales (Palumbi et al. 2003, Young et al. 2015, Carr et al. 2017). Species with strong site fidelity, however, are typically characterized by population structures with strong spatial patterns of genetic differentiation (Meylan et al. 1990, Rooker et al. 2008, Campbell et al. 2008, Bonanomi et al. 2016). This is often due to natal site fidelity where an animal either remains at its natal location (philopatry) or returns to reproduce at its natal location after an initial migration away (natal homing). But spatial population structure can also arise through foraging site fidelity to non-natal locations by juveniles or adults (Lowther et al. 2012).

Sometimes, however, diverse taxa, ranging from birds (Milot et al. 2008, Pearce et al. 2008) to fishes with varied life histories, exhibit little genetic differentiation across broad spatial scales despite natal homing (Thorrold et al. 2001), site fidelity (Whitney et al. 2012, Klein et al. 2021), or sedentary behavior of adults (van Herwerden et al. 2009, Berry et al. 2012, Gardner et al. 2015, Antoni & Saillant 2017). This can lead to a perceived mismatch in the scale of demographic connectivity, which considers exchange of individuals between populations, and estimates of geneflow (Weersing & Toonen 2009, Lowe & Allendorf 2010, Selkoe et al. 2016, Legrand et al. 2022). Such is the case for Scamp (*Mycteroperca phenax*), an economically important reef-associated grouper that is found throughout the continental shelf off the southeastern United States (U.S.) – from the northwest Gulf of Mexico to the Atlantic Ocean near North Carolina (Smith 1971, Bullock & Smith 1991, Bacheler & Ballenger 2018).

Scamp form spawning aggregations (<100 individuals) in high relief rocky areas along the edge of the continental shelf (Coleman et al. 2011, SAFMC 2013, Farmer et al. 2017, Gruss et al. 2018, Heyman et al. 2019) that are thought to comprise both resident and transient individuals (Biggs et al. 2021). The details are not well established, but compared to other aggregating grouper, like gag (*Mycteroperca microlepis*), scamp aggregations are thought to be less specific to particular locations or habitat types (Coleman et al. 2011). Some localized movement to and from spawning locations on the edge of the continental shelf is likely, but there is no direct evidence of significant migration. Tag recaptures overwhelmingly find scamp within 20km of their release location with only a handful of documented individuals traveling farther (Wilson & Burns 1996, Coleman et al. 2011, Addis et al. 2013, SEDAR 2020).

Nonetheless, genetic analyses of scamp find no spatial patterns of differentiation or population structure. Instead, a single genetic population spans the continental shelf off the southeast United States, including the Gulf and Atlantic regions (Zatcoff et al. 2004, SEDAR 2020). This has led to speculation about the mechanism of mixing that maintains genetic homogeneity across the scamp population, despite high site fidelity and little post-settlement movement.

One plausible explanation is that long distance larval dispersal by ocean currents facilitates connectivity between disparate and otherwise isolated populations (Zatcoff et al. 2004). Indeed, larval dispersal has long been implicated as a source of population connectivity in fishes (Cowen et al. 2003). For taxa with long pelagic larval durations (PLD), such as grouper (Lindeman et al. 2000), it may serve as the dominant form of connectivity. The dispersal distances required to mix scamp populations in the Gulf of Mexico with those in the Atlantic, however, are orders of magnitude greater than what is commonly assumed to be realized (Cowen

et al. 2006, Abesamis et al. 2017, Almany et al. 2017, D'Aloia et al. 2022). Moreover, the dispersal patterns of reef-fish larvae, including for grouper species, are widely thought to be dominated by self-recruitment, with most larvae settling close to where they spawned (Jones et al. 1999, Jones et al. 2005, Cowen et al. 2006, Buston et al. 2012, Almany et al. 2013, D'Aloia et al. 2015).

In U.S. waters scamp are managed as two separate stocks. One in the Gulf of Mexico, which is managed by the Gulf of Mexico Fishery Management Council and was recently estimated to be not overfished and not subject to overfishing (SEDAR 2022a), and another in the Atlantic, which is managed by the South Atlantic Fishery Management Council and was recently estimated to be overfished but not subject to overfishing (SEDAR 2022b). This two-stock structure is due, in part, to geographical boundaries, as well as a presumed biological separation between populations. In effect, this treats U.S. scamp in the Gulf of Mexico and Atlantic as two independent and homogeneous populations. If, however, sufficient larval dispersal exists to mix scamp populations in the two regions, then it could also have implications for fishery management.

In particular, spatial management decisions, like the placement of stock boundaries and Marine Protected Areas, benefit from understanding which areas provide recruitment to the broader region, and which areas rely on external recruitment (Dubois et al. 2016). These so called "source-sink" dynamics can be quantified by simultaneously considering a variety of connectivity metrics, including some that consider the retention of locally spawned larvae and others that consider the exchange of larvae between areas (Dubois et al. 2016). Moreover, understanding dispersal could influence the way recruitment is modeled during stock assessment. For example, in some instances, statistical models that include connectivity metrics better predict

109 inter-annual recruitment deviations than conventional spawner-recruit relationships do (Hidalgo
110 et al. 2019).

111 Therefore, to investigate the scale of scamp connectivity, we used an individual-based
112 model to simulate dispersal and examine the resulting recruitment dynamics. Specifically, we
113 used the open-source particle tracking platform, Connectivity Modeling System (CMS, Paris et
114 al. 2013), which combines reproductive ecology and larval biology with models of oceanic
115 currents, to transport virtual larvae through time and space. Within CMS we modeled scamp life
116 history, released virtual larvae from spawning locations throughout U.S. waters, and tracked their
117 simulated movements from spawning grounds to settlement locations. These simulations can
118 inform the degree of connectivity between fishery management units (Le Corre et al. 2018, Zeng
119 et al. 2018, Le Corre 2020), and we focused on three topics: 1) whether oceanographic
120 conditions in the region favor local retention or long-distance dispersal; 2) which spawning
121 regions are likely to produce significant scamp recruitment; and 3) the degree of trans-boundary
122 connectivity between the scamp stock units in the U.S. Gulf of Mexico and Atlantic Ocean.

123

124 ## 2. MATERIALS & METHODS

125 ### 2.1 Biophysical modeling framework

126 We used the Connectivity Modeling System (CMS) to simulate the spawning of virtual
127 eggs from expected scamp spawning locations throughout the U.S. Gulf of Mexico and Atlantic
128 regions. CMS uses the output from oceanographic models to advect individual virtual larvae
129 through time and space and monitors the trajectories of those larvae from spawning to
130 settlement. In total, we conducted eight different simulations, which used the same seasonal and

spatial spawning distributions, but differed in terms of the underlying ocean velocity fields and assumed larval traits and behaviors (Table 1). These eight simulations can be thought of as one base simulation and seven variations that explore two kinds of known uncertainty, that due to ocean circulation and that due to larval biology. In the subsequent sections we describe the configuration of the base simulation we used to model scamp dispersal. Then, we describe how we modified this base simulation to investigate hydrodynamic and biological uncertainties, and the ensemble modeling approach we used to analyze the results and quantify scamp connectivity.

2.2 Initial conditions of the base biological model

Spawning time

To determine the timing of simulated spawning in CMS we used a generalized additive model (GAM) to analyze the seasonality of all available reproductive histology data for scamp caught in the U.S. Gulf of Mexico (1972-2017, National Marine Fisheries Service – Southeast Fisheries Science Center) and Atlantic (1976-2018, South Carolina Department of Marine Resources). After removing data without reliable positional information, and years with fewer than 30 samples, these data included 5,093 reproductive samples (Figure S1, Table S1). Of these, 650 were obtained from females within approximately 24 hours of spawning, with spawning observed at depths between 14 and 177 meters. We used a binomial GAM to predict the probability that a sample came from a spawning female (η, Equations 1-3). The covariates we considered included average bottom depth (d), local change in bottom depth (delta), distance to the continental shelf-break (dist, Appendix 1 in the Supplementary Materials), day of year (doy), year (y), and whether the sample came from a fishery dependent or fishery independent source

153 (source). We calculated the depth-based covariates from the Coastal Relief Model (National
154 Geophysical Data Center) using a 100-meter radius around each catch location. Scamp are
155 thought to spawn preferentially at high relief rocky areas near the edge of the continental shelf
156 (Coleman et al. 2011, SAFMC 2013, Farmer et al. 2017, Grüss et al. 2018), but unfortunately,
157 habitat, relief and substrate data are not consistently available throughout our full study area.
158 Because these data are only available at select sites, we could not include them explicitly in this
159 model. Instead, we used the change in depth within 100-meters of each sample location as a
160 proxy for local relief.

161

162 $$\eta \sim Bernoulli(\pi), \quad (1)$$

163 $$E(\eta) = \pi, \text{ and } var(\eta) = \pi \times (1 - \pi), \quad (2)$$

164

165 $$logit(\pi) = \alpha + s_1(doy^*) + s_2(dist^\dagger) + s_3(d^\dagger) + s_4(\log(delta^\dagger)) + f_1(y) + f_2(source)$$

166 (3)

167

168 where:

169 π is the probability of a spawning female, and $(1 - \pi)$ is the probability of a male or
170 non-spawning female,

171 $logit$ is the logit link function,

172 α is the model intercept,

173 s is a smoothed cubic spline function,

174 f is a categorical function,

175 * denotes temporal covariates that changed when predicting the spawning season, and

176 † denotes spatial covariates that changed when predicting the spawning distribution.

177

178 For this, and all subsequent GAMs, we used the "mgcv" package (Wood 2011) in R (R
179 Core Team 2023). We estimated smoothing parameters using Restricted Maximum Likelihood
180 (REML) and conducted variable selection with the "select == TRUE" argument, which is the
181 recommended method for GAMs and adds an additional penalty to each term so that they can be
182 removed from the model during the fitting process (Marra & Wood 2011). The final model
183 (Equation 3) retained all variables and explained 45.1 percent of the deviance in spawning with
184 an adjusted r^2 of 0.402. This model predicted a high probability of spawning from March through
185 May, with a peak in April (Figure 1A), which is consistent with previous reports of the scamp
186 spawning season (Harris et al. 2002, Lombardi-Carlson et al. 2012, Farmer et al. 2017).

187 There is not sufficient histology sampling to estimate a different spawning season for
188 each year (Table S1), so we used this average seasonality to distribute simulated spawning
189 events throughout the year. First, we delineated the spawning season by calculating the middle
190 95% of the area under the spawning season curve from the model (Figure 1A) and only
191 simulated scamp spawning between day of year 55 (late February) and 165 (mid-June). Then,
192 within this spawning season we simulated spawning every other day and scaled the number of
193 virtual eggs spawned on each day to be proportional to the predicted probability of spawning on
194 that day. In this way, we simulated more spawning in April, when our model and other reports

suggest scamp spawning is higher, than at the beginning or end of the estimated spawning season.

Spawning location

We used a similar approach to scale the spatial distribution of simulated spawning throughout the U.S. Gulf of Mexico and Atlantic. Briefly, at grid of locations spaced at 10 km intervals, we calculated the expected spawning (λ) as the product of spatial predictions from three statistical models (Equation 4): the probability of scamp presence, the estimated abundance when present, and the probability of spawning when present. Then, we simulated spawning at each grid location, but spawned more virtual larvae at locations where these models predicted higher spawning (Figure 1B).

$$\lambda = \beta \times \mu \times \eta \quad (4)$$

where:

λ is the estimated scamp spawning

β is the probability of scamp presence

μ is the estimated scamp abundance, when present

η is the probability of scamp spawning, when present (Equation 3)

In effect, this builds a species distribution map and then uses the histology-based spawning model we described above (Equation 3) to adjust where the simulated spawning is concentrated with respect to depth, local change in depth (a proxy for local relief), and proximity

to the edge of the continental shelf. Therefore, if scamp tend to spawn closer to the shelf-edge, or at different depths than the species distribution in general, our modeling approach can readily account for this.

To build the species distribution map we used a common delta-model approach (also known as a hurdle-model) to analyze recent data (2011-2017) from five fishery independent surveys (Appendix 2, Supplementary Materials, for full details). Sampling for these surveys occurs largely from May through August, so it does not perfectly align with the scamp spawning season (March through May). However, these are the best available data to inform the relative abundance of scamp throughout U.S. waters, which is necessary to appropriately scale the magnitude of simulated spawning. Moreover, there is no evidence that scamp travel long distances to spawn, and by including a histology model, our approach accounted for potential inshore-offshore shifts in the spawning distribution compared to the species distribution.

The delta-model approach we used to estimate the species distribution map included two GAMs: a binomial sub-model that predicted the probability of scamp presence (β, Equations 5-7), and a Gaussian sub-model that predicted scamp abundance when present (μ, Equation 8). Both sub-models had the same set of covariates, which included all covariates that overlapped across the surveys: average bottom depth (d), local change in bottom depth (delta) as a proxy for local relief, distance to the shelf break (dist, Appendix 1 in the Supplementary Materials), position along the shelf break (pos, Appendix 1 in the Supplementary Materials), percent observed substrate (sub), observed maximum relief (rel), year (y), and survey program (survey).

$$\beta \sim Bernoulli(\theta) \quad (5)$$

$$E(\beta) = \theta \text{ and } var(\beta) = \theta \times (1 - \theta) \quad (6)$$

$$logit(\theta) = \alpha + s_1(dist^{\dagger}) + s_2(pos^{\dagger}) + s_3(d^{\dagger}) + s_4(\log(delta^{\dagger})) + s_5(sub) + f_1(y) + f_2(survey) + f_3(rel) \quad (7)$$

$$\sqrt[4]{\mu} = \alpha + s_1(dist^{\dagger}) + s_2(pos^{\dagger}) + s_3(d^{\dagger}) + s_4(\log(delta^{\dagger})) + s_5(sub) + f_1(y) + f_2(survey) + f_3(rel) \quad (8)$$

where:

θ is the probability of scamp presence, and $(1 - \theta)$ is the probability of absence,

equation (7) uses all visual survey data to predict the probability of scamp presence, and

equation (8) uses 4th root transformed positive count data and a gaussian error distribution to estimate scamp abundance when present.

The binomial sub-model explained 25.6% of the deviance in whether a survey observed scamp with an adjusted r^2 of 0.238. The gaussian sub-model explained 26.2% of the deviance in survey counts (when scamp were present) with an adjusted r^2 of 0.254.

We used the spatial predictions of these two sub-models, in combination with the spatial predictions from the previously described histology model (Equation 3), to estimate the spatial distribution of scamp spawning (Figure 1B). Specifically, we generated a grid of locations spaced at 10-kilometer intervals throughout the U.S. Gulf of Mexico and Atlantic and at each

location we used the spatial covariates in each model (e.g. depth, denoted by †) to predict the probability of scamp presence (β, Equations 5-7), the scamp abundance when present (μ, Equation 8), and the probability of scamp spawning when present (η, Equation 3). The product of these three predictions (Equation 4) estimates the relative amount of scamp spawning at each grid location. These models suggest that scamp are most likely to spawn around 75 meters of depth (Figure S5) and at locations near the edge of the continental shelf (Figure 1B), which is consistent with previous reports of scamp spawning (Coleman et al. 2011, SAFMC 2013, Farmer et al. 2017, Grüss et al. 2018).

Unfortunately, observations of relief and substrate are not available throughout our full study area. Therefore, we could not include these spatial covariates in our spawning model or use them to predict the species distribution. Instead, we used the local change in depth within a 100-meter radius of each location as a proxy for local relief. In addition, we used the survey observations of percent available substrate and maximum relief as controlling variables in our species distribution modeling to better estimate the relationship between scamp abundance and the other spatial covariates in the model (e.g. depth). Therefore, our spatial models likely captured the broad spatial patterns in scamp spawning, but they cannot account for spatial variation at fine scales.

In addition, there is not enough empirical data to estimate annual spawning maps. Instead, we used data from multiple years to inform an average spatial distribution that we applied for all simulation years. This average distribution analyzed recent survey data to estimate the relative abundance of scamp and combined it with histology samples that were collected over a longer time-period. Therefore, the exact spawning locations of scamp and how they might change over time, remain uncertain.

To confine the spatial extent of spawning locations we calculated the middle 95% of the area under the depth marginal effect of all three models combined (Figure S5). As a result, we simulated spawning at grid locations with an average depth between 14 and 279 meters. Then, we scaled the number of virtual eggs spawned at each grid location to be proportional to the predicted probability of spawning at that location (Figure 1B), which was highest near the edge of the continental shelf. This is consistent with previous reports (Coleman et al. 2011, SAFMC 2013, Farmer et al. 2017, Grüss et al. 2018) and the empirical depth range of spawning observed in the histology data (14 to 177 meters, with most spawning between 50 and 100 meters).

Scaling the magnitude of spawning

In each year, we simulated approximately 100,000 virtual eggs, a number we chose through a resampling analysis of preliminary results (Appendix 3 in the Supplementary Materials). To calculate the number of eggs spawned at each time and place we first used the histology model (Equation 3) to distribute the 100,000 eggs throughout the spawning season (Figure 1A). Then, on each spawning day we used the spatial distribution (Figure 1B) based on all three models combined (Equation 4) to allocate the eggs to each grid location. Finally, we rounded the number of eggs for each spawning event (combination of time and place) to the nearest whole number. After rounding, we simulated 99,102 eggs per year and used the same temporal and spatial distribution for each year of our eight simulations (base and seven sensitivity simulations). In total, we simulated the spawning of 3,765,876 virtual eggs.

We simulated spawning every other day during the spawning season, but for computational efficiency we did not spawn eggs from all locations every time. Instead, we randomly assigned spawning locations to one of five groups and spawned eggs from each group on a different set of dates (Figure S7). For example, at locations in one group we simulated

303 spawning on days of year 55, 65, 75, etc., but at nearby locations in another group we simulated
304 spawning on days of year 57, 67, 77, etc. In this way, only 20% of the locations simulated
305 spawning on each day, with spawning occurring at individual locations every 10 days. This
306 approach maintained the temporal and spatial resolution needed for robust probabilistic results
307 but reduced the total number of virtual eggs required for each simulation, which is important for
308 computational efficiency.

309 *Vertical distribution of eggs and larvae*

310 We simulated spawning 10 meters above the sea floor, which is consistent with the depth
311 range in which scamp courtship behavior has been observed (Gilmore & Jones 1992, Schobernd
312 & Sedberry 2009). Immediately after spawning the simulated eggs float to the surface, as is
313 consistent with grouper eggs. The exact rate that scamp eggs float is unknown, so we specified
314 that simulated eggs float to the surface over the first 9 hours and then remain in the top 15 meters
315 of the water column until they hatch. We defined this assumption through a series of initial
316 simulations that also confirmed that the resulting connectivity patterns were similar under a wide
317 range of buoyancy assumptions (Appendix 4). After two days, when grouper eggs typically hatch
318 (Roberts & Schleider 1983, Colin et al. 1996), the simulated larvae undergo vertical migration
319 with depths determined probabilistically (Table 2). For the base simulation we used one vertical
320 distribution throughout the entire larval duration (Table 2: "No Ontogenetic Shift"). We
321 informed the assumed vertical distribution of simulated larvae by analyzing the limited empirical
322 data available for grouper larvae caught during the scamp spawning season (Appendix 4 in the
323 Supplementary Materials). Because these data are limited, however, the exact vertical
324 distribution of scamp larvae is uncertain.

325 *Settlement*

We only allowed virtual larvae to settle successfully when certain criteria were met. First, we specified the settlement competency period from 33 to 52 days. Because the pelagic larval duration (PLD) of scamp remains unknown, we approximated it using information on congeneric gag grouper (*M. microlepis*) larvae in the study region (Fitzhugh et al. 2005, Adamski et al. 2012), which tend to settle between 33 and 52 days of age (Appendix 5 in the Supplementary Materials). These values are also consistent with the PLD of another closely related species, black grouper (*M. bonaci*, Keener et al. 1988).

Second, we used 30 meters as a boundary for suitable settlement habitat (see below) and only considered virtual larvae to have successfully settled if they reached a depth less than 30 meters when they were between 33 and 52 days old. If a simulated larva reached 33 days old and was not in suitable settlement habitat (i.e., depth <30m), then it continued to move until it either encountered settlement habitat or it reached the maximum PLD (52 days), at which point it stopped and we considered it dead.

Little is known about the settlement preferences of scamp, but larvae are not known to require a specific nursery habitat and juveniles are thought to inhabit reefs between 20m and 30m of depth (Coleman et al. 2011). This is consistent with the few data available for age zero and age one scamp caught in the northeastern Gulf of Mexico, which suggest that young scamp are predominantly caught at depths less than 30 meters (Figure S9). In addition, surveys that sample depths less than 30 meters, like those in the Florida Keys (Keller et al. 2020), tend to see a higher proportion of small scamp than do surveys that operate in deeper waters (Thompson et al. 2020). Therefore, we felt that using a depth-based settlement criteria of 30 meters was appropriate.

348 To delineate settlement habitat, we extracted the 0- and 30-meter isobaths from the global
349 30 arc-second bathymetry grid available from GEBCO (General Bathymetric Chart of the
350 Oceans, www.gebco.net) and defined suitable settlement habitat as all areas between these
351 isobaths on the U.S. Gulf and Atlantic continental shelves. This does not account for potential
352 spatiotemporal variation in settlement habitat, which is not well understood for scamp and
353 beyond the scope of this study. It also assumes that scamp larvae can either settle anywhere
354 shallower than 30 meters, or that once near preferred settlement habitat (yet unknown) larvae can
355 direct their swimming to increase the likelihood of finding it. These are reasonable assumptions
356 given the lack of information on scamp settlement and that many fish larvae can alter their
357 behavior to facilitate settlement (Montgomery et al. 2001, Kingsford et al. 2002, Gerlach et al.
358 2006, Botesch et al. 2016, Teodósio et al. 2016, Faillettaz et al. 2018).

359 Hereafter we use terms such as settlement, successful larvae, and settlers to refer to
360 virtual larvae that found suitable settlement habitat during the competency period instead of
361 reaching their maximum PLD in deeper waters. Similarly, for fluency, we sometimes use terms
362 like recruit or recruitment interchangeably with settler or settlement, even though our simulations
363 do not model post-settlement processes that influence whether settled larvae ultimately recruit to
364 the population as juveniles.

365

366

367 2.3 Exploring known uncertainties

368 There are several sources of uncertainty that we know will influence the trajectories of
369 simulated larvae, and therefore, our estimates of scamp connectivity. Different hydrodynamic

models produce different current velocity estimates, and several areas of scamp larval ecology are relatively understudied. Therefore, we conducted seven additional simulations that use alternative assumptions for the ocean velocity estimates, pelagic larval duration, settlement habitat, and vertical distribution of larvae. These are analogous to sensitivity analyses often used in stock assessment, or robustness trials often discussed for Management Strategy Evaluation (Punt et al. 2016).

Ocean velocity fields

A large source of uncertainty for simulating larval dispersal is the variability between the estimated velocity fields from different hydrodynamic products (Karnauskas et al. 2022). Therefore, we conducted five simulations, including the base simulation, that assumed the same biological parameterization described above (i.e., spawning distribution, vertical distribution of eggs and larvae, and settlement criteria), but used velocity fields from different hydrodynamic products to transport the simulated larvae.

In total, we used velocity fields from six hydrodynamic products, but one was only used as a nest for others that did not cover our entire study area. These products were obtained from different ocean circulation models as well as implementations with a range of spatial and temporal resolutions, forcings, and data assimilation approaches (summarized in Table 3, details in Appendix 6). Note that we do not prefer any hydrodynamic model over the others. Instead, we gave them equal weight when analyzing our results (see *Ensemble models* below) and only refer to a base simulation for clarity in describing our methods.

Briefly, we used velocity fields from 1) the Hybrid Coordinate Ocean Model (HYCOM) Gulf of Mexico 1/25° analysis (hereafter GOM HYCOM), 2) the HYCOM Gulf of Mexico 1/50°

analysis (hereafter GOM HYCOM HiRes, Le Hénaff & Kourafalou 2016), 3) the HYCOM Intra-American Seas 1/32° analysis (hereafter HYCOM IAS), 4) the Mercator GLORYS12V1 1/12° reanalysis (hereafter Mercator, Lellouche et al. 2021), and 5) the South Atlantic Bight and Gulf of Mexico 1/25° model (hereafter SABGOM, Hyun & He 2010, Xue et al. 2015). Two velocity fields (GOM HYCOM and GOM HYCOM HiRes) do not extend north of 32°N. Therefore, to cover our entire study area we nested them within 6) the operational 1/12° global HYCOM Global Ocean Forecasting System (hereafter HYCOM GOFS, Chassignet et al. 2007), which provides the boundary conditions for both GOM HYCOM and GOM HYCOM HiRes. For all hydrodynamic products we used velocity fields at daily intervals.

Each product is available for different years and thus, simulations using individual velocity fields do not always overlap (Table 3). However, the purpose of this study is to estimate probabilistic connectivity and recruitment patterns over time, not to produce a hindcast of recruitment in specific years. Therefore, we aimed to capture the interannual variability within each hydrodynamic product by using at least 5 years of velocity fields (except for HYCOM IAS). This ensured that our results were probabilistically robust and allowed us to compare the general connectivity trends from simulations that use non-overlapping years (Karnauskas et al. 2022).

To account for processes not resolved by the resolution of the hydrodynamic products (sub-grid scales) we used the random walk displacement algorithm in CMS. It adds a random component to the motion of virtual larvae and approximates diffusion. The diffusivity values we used to scale the random walk ranged from 12 m^2/s to 20 m^2/s with the value depending on the horizontal resolution of the ocean velocity field and Okubo's (1971) parameterization. However, SABGOM has lower eddy kinetic energy, and therefore variability, than other models (Figure

S10). So, after unpublished sensitivity explorations by Karnauskas et al. (2022), we used a slightly higher diffusivity value for SABGOM than for other models with the same horizontal resolution to ensure that our results captured a probabilistic distribution of dispersal pathways.

Biological traits

There is also uncertainty in several aspects of scamp larval biology and behavior. Specifically, little is known about the pelagic larval duration of scamp, how the vertical distribution of scamp larvae changes throughout ontogeny, or the preferred settlement habitat of scamp. However, in contrast to the hydrodynamic models, of which none are preferred, the base model (described above) does in fact represent our best assessment of the relevant scamp biology and behavior. To investigate how uncertainty in these traits might influence our results we conducted three additional simulations that vary each trait, one at a time (Table 1). One extended the PLD to 57 days, which is the 97.5% quantile of settlement age for gag larvae in the Atlantic (Adamski et al. 2012). The second incorporated an ontogenetic shift in the vertical distribution of larvae (Table 2: "Ontogenetic Shift"). The third expanded the settlement criteria to 45 meters. All four simulations (base and three biological variations) used the same temporal and spatial spawning distribution as well as the same ocean velocity fields (GOM HYCOM nested within GOFS).

2.4 Data analysis

Metrics and plots

To investigate the general patterns of scamp connectivity we used two graphical approaches. First, we visualized connectivity matrices, which aggregate successfully settled

larvae based on where they spawned and where they settled (Figure 2). These plots provide a convenient way to determine whether most larvae are likely to settle close to where they started (i.e., local retention as defined by Botsford et al. 2009) or disperse longer distances. Second, we mapped the spatial distribution of where successfully settled larvae spawned and settled (Figure 3). These maps help to identify important spawning locations that are likely to be strong sources of recruitment to the broader region, and settlement locations that are likely to be recruitment hotspots and collect larvae from widespread spawning locations.

In addition to these general patterns of connectivity, we specifically focus on the connectivity dynamics between the U.S. Gulf of Mexico and Atlantic regions. To delineate the two regions, we used the jurisdictions of the Gulf of Mexico and South Atlantic Fisheries Management Councils. Because the jurisdictions of these management bodies do not apply within state waters (three nautical miles from shore), we approximated a boundary between them in a way that can be applied to any location, including those within state waters. Our boundary (shown in Figure 1B) follows U.S. Highway 1 from Miami, Florida, to Key West, Florida, until it intersects latitude 24° 35’ N, which it follows west until it intersects longitude 83° W, which it follows south. We considered all spawning and settlement habitat north and west of this line to be in the Gulf of Mexico and all habitat south and east of this line to be in the Atlantic. We also further partitioned the U.S. Atlantic into subregions at latitude 25.75° N (approximately Miami, Florida) and latitude 28.5° N (approximately Cape Canaveral, Florida). Using these geographic boundaries, we calculated a set of proportions to describe the trans-regional connectivity patterns in the area, including what percent of recruits settling in the Atlantic came from the Gulf of Mexico.

Ensemble models

460 In general, we report the findings of a hydrodynamic ensemble, a biological ensemble,
461 and an overall ensemble. The hydrodynamic ensemble combines and summarizes the results of
462 five simulations: the base simulation and the four variations that change the underlying ocean
463 velocity field. The biological ensemble combines and summarizes the results of four simulations:
464 the base simulation and the three variations that change the larval biology and behavior. The
465 overall ensemble combines and summarizes the results of all eight simulations together.

466 For the connectivity matrix plots, which use spatial polygons (Figure S11) to aggregate
467 successful recruits, and the raster maps, we first calculated the result of interest (e.g., number of
468 successfully settled particles spawned in a particular area) for each simulation and normalized it
469 by the total number of virtual larvae spawned in the same simulation (Equation 9). Then, for
470 each raster cell or matrix element, we calculated the arithmetic mean across the simulations in
471 each ensemble (Equation 10). Finally, for plotting, we normalized the mean values so that they
472 are proportional to the maximum.

473 (9)

474 $$N_s[i,j] = \frac{\sum n_{s,i,j}}{T_s}$$

475 where:

476 $$n_{s,i,j} = \begin{cases} \text{Recruits spawned in polygon } i \text{ and settled in polygon } j \text{ for simulation } s \text{ (Fig. 2)} \\ \text{Recruits spawned from raster cell } [i,j] \text{ for simulation } s \text{ (Fig. 3A)} \\ \text{Recruits settled in raster cell } [i,j] \text{ for simulation } s \text{ (Fig. 3B)} \end{cases}$$

477 T_s is the total number of larvae spawned in simulation s

478 (10)

479 $$\overline{N_E}[i,j] = \frac{1}{k_E}\sum_{s \in E} N_s[i,j]$$

480 where:

481 E is an ensemble of simulations,

482 k_E is the number of simulations in the ensemble

483

484 For the proportions (e.g., percentage of Atlantic recruits from Gulf of Mexico spawning
485 areas), we resampled each simulation 1000 times and calculated every proportion for each
486 resample. Then, we pooled the resampled proportions from all the simulations in an ensemble
487 before calculating the ensemble mean and standard deviation. This captures the uncertainty
488 within each simulation as well as across the simulations in an ensemble. We also, however,
489 examined the results for each simulation individually and highlight major differences when
490 relevant.

491

492 3. RESULTS

493 On broad spatial scales we found a predominant pattern of local retention (Botsford et al.
494 2009), with most settled larvae ending near their spawning location (Figure 2). Across all
495 simulations, most potential recruits (i.e., virtual larvae that found settlement habitat) started in
496 the eastern Gulf of Mexico (Figure 3A), with a peak off the west coast of Florida near 28° N.
497 This area was also the most successful settlement area, with the highest number of potential
498 recruits settling off the west coast of Florida near 28° N (Figure 3B). In general, the high degree
499 of local retention persisted across all eight simulations (Figure S12), but the spawning and
500 settlement locations of potential recruits were more spatially distributed across the northern Gulf

501 of Mexico when the results were summarized over the simulations in the hydrodynamic
502 ensemble than when summarized over the simulations in the biological ensemble (Figures S13
503 and S14).

504 Despite this trend of high local retention, we also found that more than one-third of
505 virtual scamp larvae settling in the U.S. Atlantic region came from the Gulf of Mexico (Figure
506 4). Almost 65% of these larvae, which were transported from the Gulf to the Atlantic, settled in
507 the Florida Keys – technically in the Atlantic, but very close to the boundary between the two
508 regions. To more conservatively estimate the contribution that Gulf of Mexico spawning makes
509 to recruitment in the Atlantic, we also report the results when we only consider those potential
510 recruits that settled farther into the Atlantic (i.e., north of latitude 25.75° N, or north of latitude
511 28.5° N). Even then, 17% of the larvae that settled north of latitude 25.75° N (Miami), and 10%
512 of the larvae that settled north of latitude 28.5° N (Cape Canaveral), started in the Gulf of
513 Mexico (Table 4). There is, however, considerable variation in these proportions, both between
514 simulations and between years within a simulation (Table 4, Figure 5).

515 The percentage of potential Atlantic recruits (i.e., virtual larvae that settled anywhere in
516 the Atlantic) that came from the Gulf of Mexico is sensitive to the biological parameterization of
517 our simulations (e.g., PLD, settlement criteria, vertical distribution). The differences are greater,
518 however, when we compare simulations that use the same biological parameterization but rely on
519 current velocity estimates from different oceanographic models. For example, the simulation
520 using SABGOM estimated that 19% of potential Atlantic recruits started in the Gulf (year-to-
521 year values range from 12 to 35%, Table 5), while the simulation using the high resolution
522 HYCOM model estimated that 56% of potential Atlantic recruits started in the Gulf (year to year
523 values range from 29 to 74%, Table 5). On the other hand, the values from simulations in the

biological ensemble, which all use the same hydrodynamic model, only range from 29 to 43%. There is still, however, considerable year to year variability within each simulation (Figure 5).

This relationship changes when we focus on larvae that settled farther north in the Atlantic. Specifically, the percentage of potential Atlantic recruits that settled north of latitude 28.5° N (Cape Canaveral) but came from the Gulf is more sensitive to the biological specifications of a simulation than to the hydrodynamic model used. For example, in the base simulation 10% of larvae that settled north of Cape Canaveral started in the Gulf of Mexico. However, when the suitable settlement habitat was extended from depths less than 30 meters to depths less than 45 meters, 28% of the larvae that settled north of Cape Canaveral came from the Gulf of Mexico. By contrast, the percent of potential recruits north of Cape Canaveral that came from the Gulf remained relatively consistent across the simulations in the hydrodynamic ensemble, which all used the same biological parameterization as the base simulation (2-10%; Table 4).

Larvae that leave the Gulf of Mexico and settle in the Atlantic came overwhelmingly from the West Florida Shelf (Figure 6). When we focus only on potential recruits that settle farther into the Atlantic, north of latitude 25.75° N (Miami), the spawning locations of these trans-regional settlers were limited largely to the southern portion of the West Florida Shelf. This southern concentration is even more extreme when we focus only on potential recruits that settle north of latitude 28.5° N (Cape Canaveral).

4. DISCUSSION

545 Consistent with expectation (Jones et al. 2005, Cowen et al. 2006, Buston et al. 2011,
546 Almany et al. 2013, Vaz et al. 2023), we found that scamp dispersal largely followed a pattern of
547 local retention (Figure 2). Most virtual larvae in our simulations settled close to their spawning
548 sites. However, there was also a consistent pattern of some larvae dispersing away from the natal
549 place. Notably, although most larvae from the West Florida Shelf settled there, some dispersed to
550 the Florida Keys and along the Atlantic shelf, even as far north as North Carolina (Figure 2).
551 Even if not predominant, this pattern of consistent long-distance dispersal has important
552 ramifications for the connectivity dynamics, genetic structure, and fishery management of
553 scamp.

554 Specifically, we found that approximately one third of potential scamp recruits to the
555 Atlantic came from the Gulf of Mexico (Figure 4). Most of these recruits that left the Gulf of
556 Mexico settled in the Florida Keys, but even when we only considered potential Atlantic recruits
557 settling north of latitude 25.75° N (Miami, Florida), Gulf of Mexico spawning still accounted for
558 17% of Atlantic recruitment. This external recruitment might increase the resilience of the scamp
559 population in the U.S. Atlantic. In addition, this degree of connectivity appears to provide
560 sufficient trans-regional mixing to minimize spatial patterns in the genetic structure of scamp
561 populations (Zatcoff et al. 2004).

562 It is important to note that demographic connectivity examines unique events of
563 individuals moving between regions, while genetic connectivity studies unveil patterns that occur
564 over multiple generations and evolutionary timescales (Carr et al. 2017, Legrand et al., 2022,
565 Vaz et al. 2022). Our results suggest a recurring pattern of transport from the Gulf of Mexico to
566 the Atlantic Ocean, which, if consistent over long timescales, can explain the observed genetic
567 structure of scamp populations in the region. Particularly, if we consider the possibility of multi-

568 generational transport, which has been shown to better predict spatial patterns in genetic
569 differentiation than single-generation transport models or conventional conceptual models like
570 isolation-by-distance (Legrand et al., 2022).

571 Dispersal over multiple generations can magnify the effects of demographic connectivity
572 and reconcile mismatches in the spatial scale of demographic and genetic connectivity through
573 two mechanisms (Legrand et al., 2022). Filial connectivity traces explicit connections between
574 parents and offspring (i.e., dispersal of single lineages over generations). Coalescent connectivity
575 considers the implicit linkages between areas that have no demographic connectivity between
576 them but share common ancestry because they receive dispersal from the same external area.
577 Both filial and coalescent connectivity are important when considering how demographic
578 connectivity pathways revealed by dispersal modeling may lead to observed patterns of genetic
579 connectivity (Legrand et al., 2022).

580 For example, even if a particular individual doesn't move from the Gulf to the Atlantic, it
581 may disperse downstream far enough such that when it reproduces as an adult its own larvae are
582 more likely to move between the regions. Specifically, most potential Atlantic recruits from the
583 Gulf of Mexico started on the West Florida Shelf, but there is also dispersal from the Florida
584 Panhandle to the West Florida Shelf. Therefore, the West Florida Shelf may serve as a stepping-
585 stone that facilitates filial connectivity (Legrand et al., 2022) between scamp near the Florida
586 Panhandle and those in the Atlantic. In addition, because there is also dispersal from the Florida
587 Panhandle to Louisiana, there may be coalescent connectivity (Legrand et al., 2022) between
588 scamp in Louisiana and the Atlantic because they share common ancestors (i.e., spawners near
589 the Florida Panhandle). Thus, under the conceptual framework outlined by Legrand et al. (2022),

590 the connectivity pathways revealed by our simulations could lead to broad spatial mixing among
591 the scamp throughout the Gulf of Mexico and U.S. Atlantic.

592 That such a large proportion of Atlantic recruitment comes from the Gulf of Mexico, even
593 though our findings generally favor a pattern of local retention, may initially seem incongruous.
594 This phenomenon likely arises, however, by the way that oceanographic transport patterns
595 overlay the scamp spawning distribution. One of the most ubiquitous circulation patterns in the
596 Gulf is the presence of the meandering Loop Current, which enters the Gulf flowing northward
597 from the Yucatan Straits, rotates clockwise, flowing eastward and then southwards along the
598 outer West Florida Shelf (Hetland et al. 1999, Le Hénaff & Kourafalou 2016). The dispersal
599 pathway connecting the Gulf and Atlantic scamp populations passes through the Straits of
600 Florida, a relatively narrow channel between Cuba and the Florida Keys. When entering the
601 Florida Straits, the Loop Current originates the eastward flowing Florida Current, which
602 dominates the Straits circulation, along with locally and remotely generated mesoscale eddies
603 also translating eastward (Le Hénaff & Kourafalou 2016). Upon exiting the Florida Straits, the
604 Florida Current joins the Gulf Stream, which flows northeastward. Thus, prevailing current
605 patterns in our study region facilitate dispersal of potential recruits from the Gulf to the Atlantic,
606 but relatively few simulated larvae were transported upstream in the Florida Straits, from the
607 Atlantic to the Gulf. As a result, larvae transported out of the Gulf of Mexico can find acceptable
608 settlement habitat in the Atlantic, but larvae transported out of the Atlantic within the Gulf
609 Stream are removed from the system entirely. For scamp, this is exacerbated by the relative
610 spawning in the two regions. Because scamp biomass is higher in the Gulf of Mexico than in the
611 Atlantic (SEDAR 2022a, SEDAR 2022b), the amount of spawning is higher as well (Figure 1B).
612 Therefore, more larvae originate in the Gulf of Mexico than in the Atlantic. When combined

613 with the observed larval dispersal pathways, this distribution leads to a large proportion of
614 potential Atlantic recruits coming from the Gulf of Mexico even though most larvae settled close
615 to their spawning grounds.

616 This set of conditions may not be geographically widespread, but that does not imply the
617 findings are limited to scamp. Even if these transport dynamics are unique to this region, the
618 results are likely applicable to an extensive set of reef-associated species that span the Gulf of
619 Mexico and U.S. South Atlantic. Indeed, results for red snapper suggest that up to one-third of
620 Atlantic recruits come from spawning areas in the Gulf of Mexico (Karnauskas et al. 2022). We
621 expect the extent of Atlantic recruitment from the Gulf of Mexico to be highest for species that
622 spawn on the West Florida Shelf, have higher biomass in the Gulf of Mexico than in the Atlantic,
623 and have extended pelagic larval durations. By contrast, the effect may be tempered in species
624 with spawning concentrations farther west in the Gulf of Mexico, or species with higher
625 abundance in the Atlantic, such as black sea bass (*Centropristis striata*).

626 This connectivity between the two regions has important implications for the assessment
627 and management of economically important species. Currently, scamp and other reef-associated
628 fishes near the southeast U.S. are assessed and managed as two distinct stocks, one in the U.S.
629 Gulf of Mexico and one in the Atlantic. For scamp, our results suggest that the two stocks are
630 connected through source-sink recruitment dynamics, with some Atlantic recruits originating in
631 the Gulf of Mexico. Considering these findings, resource managers may wish to revisit the hard
632 separation of jurisdictional regions, or if this is not feasible, recognize that management
633 decisions applied in the Gulf of Mexico will likely influence scamp abundance in the Atlantic.

634 For stock assessment, these results may inform our understanding of spawner-recruit
635 relationships and how that relationship is modeled. Ideally, the stock assessment could

636 incorporate an index of connectivity as a covariate in the recruitment model. Doing so could help
637 explain variance in annual recruitment patterns (Hidalgo et al. 2019) and improve short-term
638 forecasts if the terminal year of the assessment lags behind the terminal year of the
639 hydrodynamic models.

640 Precisely estimating annual connectivity dynamics would be helpful for stock assessment,
641 but it was not our goal. Instead, we probabilistically informed the general dispersal patterns of
642 scamp. Specifically, even though we used ocean velocity estimates for different years, all of our
643 simulations used the same seasonal and spatial spawning distributions. Similarly, we assumed
644 the same spatial settlement criteria and pelagic larval duration for all years. In reality, the
645 spatiotemporal dynamics of spawning and settlement are complex processes influenced by many
646 factors (e.g., temperature). Therefore, they are likely to change from year to year, but we did not
647 have sufficient data to model these spatiotemporal nuances. Future simulations could consider
648 exploring annual variation in both spawning (e.g., Di Stefano et al., 2022*)* and settlement (e.g.,
649 Druon et al., 2015), particularly if they aim to hindcast recruitment estimates for specific years.

650 Similarly, our results must also be considered at the appropriate spatial scale. Scamp are
651 thought to form transient spawning aggregations in rocky areas with high local relief (Coleman
652 et al. 2011, SAFMC 2013, Farmer et al. 2017, Grüss et al. 2018, Heyman et al. 2019, Biggs et al.
653 2021). We included these factors, when possible (e.g., local relief from modeled bathymetry),
654 but fine-scale habitat information is not available throughout our study area and the details of
655 scamp's aggregation behavior remain uncertain. Therefore, our spatial models are likely to
656 approximate the broad spatial trends in scamp spawning, but they cannot account for fine scale
657 patterns due to habitat patchiness, local movements, or transient aggregations.

In addition, the spatial resolution of the ocean circulation models in our study area range from 2km to 8km (Table 3) so they cannot resolve flow at finer spatial scales. Consequently, the results of our dispersal simulations can probabilistically inform the general connectivity patterns expected for scamp and help to identify which spawning or settlement regions are likely important. They cannot, however, precisely identify specific spawning or settlement locations, or be used to compare neighboring locations with certainty.

To explore whether our results were robust to alternative assumptions of scamp larval biology and in ocean circulation, we conducted a suite of sensitivity analyses. The goal of these explorations was not to disentangle the relative importance of physical oceanography and larval biology on the ultimate dispersal patterns of scamp, but rather to understand how known uncertainties might influence our findings. Our general conclusions were robust to the choice of hydrodynamic model and assumed larval biology, but there was considerable quantitative variation across the simulation results.

The greatest variation was across simulations in the hydrodynamic ensemble, which used different ocean velocity fields but the same biological parameterization. For example, the simulation that relied on velocity fields from the GOM HYCOM HiRes model estimated that 56% of Atlantic recruits came from the Gulf of Mexico, while the simulation using velocity fields from the SABGOM model estimated that only 19% did (Table 5). This is consistent with results for red snapper (Karnauskas et al. 2022), which also found that SABGOM provided lower estimates of Atlantic recruitment coming from the Gulf of Mexico than other hydrodynamic models. This is most likely due to differences in the hydrodynamic models themselves, as SABGOM presented with lower variability, than other models (Karnauskas et al. 2022). This

680 variability in the flow field, which is largely due to the formation and passage of mesoscale
681 eddies, is essential to facilitate connectivity between the Gulf and Atlantic regions.

682 It is hard to completely exclude the possibility of a year effect, however, as we were
683 constrained by the years that ocean velocity estimates were available. Therefore, our SABGOM
684 simulation used an earlier set of years (2003-2010) than the other simulations, which started in or
685 after 2010. This difference in year sets can influence connectivity estimates because of
686 unpredictable changes in the state and position of the Loop Current that lead to considerable
687 year-to-year variability in the circulation patterns in the northeast Gulf of Mexico (Liu et al.
688 2016). Therefore, the degree that the Loop Current extends north into the Gulf of Mexico and the
689 seasonal timing of these intrusions are likely to change from one year to the next, which will, in
690 turn, influence the annual estimates of connectivity. However, variability in the Loop Current is
691 greatest on time scales of two years or less (Liu et al. 2016), so because we used at least five
692 years for most hydrodynamic models the results are probabilistically robust (Karnauskas et al.
693 2022). Therefore, we can compare the general patterns across simulations, even those that used
694 different years.

695 In addition, there was still considerable variation between hydrodynamic models that used
696 largely overlapping years (e.g., Mercator, HYCOM, HYCOM-HiRes). Even within a given
697 simulation year different hydrodynamic models provided different estimates of how many
698 Atlantic recruits came from the Gulf (Table 5). However, it wasn't simply that one
699 hydrodynamic model consistently provided higher estimates than another and they all followed
700 the same trend from one year to the next. Instead, there were also differences in the interannual
701 patterns between simulations that use different velocity fields (Figure 5). This is likely because

the mechanistic factors that control when and how far the Loop Current intrudes into the Gulf of Mexico are not fully understood (Weisberg & Liu 2017, National Academies of Sciences 2018).

There was less variation across the simulations in the biological ensemble, which all used the same hydrodynamic model. This does not, however, imply that variability in current velocity estimates is more important in determining dispersal patterns than variability in larval biology. Indeed, biological assumptions, like the vertical distribution of larvae in the water column, can have profound implications for the ultimate dispersal patterns (Hernández et al. 2023). In our case, the alternative biological assumptions we considered apparently presented smaller variations around the base simulation than the alternative flow representations did. Even still, changing the biological parameterization did influence our simulated recruitment dynamics (Table 4) and connectivity estimates (Table 5, Figure 5). Relative to the base simulation, increasing the PLD and extending the settlement criteria to 45 meters both increased the proportion of potential Atlantic recruits that came from the Gulf of Mexico. Conversely, incorporating ontogenetic vertical migration (OVM) decreased the proportion of potential Atlantic recruits that spawned in the Gulf. This is largely because of a decrease in the proportion of Gulf of Mexico spawned larvae that successfully settled, an increase in the proportion of Atlantic spawned larvae that successfully settled (Table 5), and a corresponding increase in local retention in the Atlantic, particularly near North Carolina (Figure S12). Not surprisingly, the variation that did exist remained consistent from one year to the next. For example, the simulation using a settlement criterion of 45-meters always resulted in the highest estimate of connectivity (Figure 5).

Research recommendations

Our findings highlight several avenues for future exploration. As suggested by Swearer et al. (2019), empirical observations could help validate our findings and confirm our assumptions. For example, our simulations estimate that approximately one-third of scamp recruitment to the U.S. Atlantic comes from the Gulf of Mexico. This result could be explored empirically through targeted genetic analysis that explores the natal origin of individual scamp in the Atlantic.

In addition, a suite of empirical sampling could target areas where our models predict high scamp spawning. This would both confirm the predictions of our spatial models, which underlie our dispersal simulations, and help to better understand the spatiotemporal dynamics of scamp spawning. Histological sampling could further inform the location and character of spawning sites, as well as whether the seasonality of spawning is consistent throughout scamp's range. Once spawning locations are identified, tagging studies could help reveal the details of transient aggregation behavior and the extent of seasonal spawning migrations, both of which remain uncertain and are likely important for management (Erisman et al. 2015, Heyman et al. 2019, Biggs et al. 2021).

Future connectivity explorations could then incorporate an updated understanding of the spatiotemporal variability in spawning as more empirical data become available. Additional dispersal simulations would also benefit from a better understanding of scamp larval ecology. The vertical distribution of scamp larvae is not well studied, and these assumptions are known to influence the results of dispersal simulations (Hernández et al. 2023). Therefore, additional ichthyoplankton sampling with refined taxonomic classification could better inform future connectivity simulations. Similarly, little is known about scamp's pelagic larval duration or nursery habitat, so we conducted sensitivity analyses to explore the robustness of our results.

Empirical studies looking at larval ingress or targeting newly settled young scamp could help inform these assumptions for future dispersal simulations.

We explored the sensitivity of our results to several sources of uncertainty, but future studies investigating connectivity between the Gulf of Mexico and Atlantic could explore others. Specifically, if those larvae that settle in the Atlantic after starting in Gulf of Mexico tend to settle later during the pelagic larval duration than other settlers, including larval mortality could influence the degree of connectivity between the two regions. Finally, diverse fish larvae are known to use a variety of environmental cues to orient their swimming (Faillettaz et al. 2015, Cresci et al. 2019, Leis et al. 2021, Berenshtein et al. 2022). Future simulations could also investigate how this potential orientation behavior might influence the expected connectivity between the Gulf of Mexico and US Atlantic.

Synthesis

Taken together, our findings provide strong evidence that episodic but consistent long-distance larval dispersal facilitates the connectivity of scamp populations on a broad spatial scale. Moreover, due to the pattern of directional oceanographic transport, and the spatial differences in abundance, this connectivity leads to the U.S. Atlantic scamp population receiving a high proportion of external potential recruits from the Gulf of Mexico. Although this may increase the resilience of the Atlantic population, it also means the sustainability of the Atlantic population may rely, in part, on the health of spawning populations in the Gulf of Mexico.

5. ACKNOWLEDGEMENTS

This work relied on many data products and we thank the following data providers: Alexandra Bozec, Eric Chassignet, and Mathieu Le Hénaff provided ocean velocity estimates; Jeremiah Blondeau, Matthew Campbell, Chris Gardner, Ted Switzer, and Kevin Thompson provided visual survey data; Linda Lombardi-Carslon, Tracey Smart, and David Wyanski provided histology data; Trika Gerard and Glenn Zapfe provided larval data; Tim MacDonald provided data on age 0 and 1 scamp. Finally, we thank Nikolai Klibansky for his insight and reviewing a draft of the manuscript, Chip Collier, Todd Kellison, and Sue Lowerre-Barbieri for helpful conversations, and three anonymous reviewers for invaluable suggestions. The scientific results and conclusions, as well as any views and opinions expressed herein, are those of the authors and do not necessarily reflect those of any government agency. The contributions by ACV were carried out under the auspices of the Cooperative Institute for Marine and Atmospheric Studies (CIMAS), a cooperative institute of the University of Miami and the National Oceanic and Atmospheric Administration, cooperative agreement #NA20OAR4320472.

786 6. LITERATURE CITED

787 Abesamis RA, Saenz-Agudelo P, Berumen ML, Bode M, Jadloc CRL, Solera LA, Villanoy CL,
788 Bernardo LPC, Alcala AC, Russ GR (2017) Reef-fish larval dispersal patterns validate
789 no-take marine reserve network connectivity that links human communities. Coral Reefs
790 36:791-801

791 Adamski KA, Buckel JA, Martin GB, Ahrenholz DW, Hare JA (2012) Fertilization dates,
792 pelagic larval durations, and growth in gag (*Mycteroperca microlepis*) from North
793 Carolina, USA. Bulletin of Marine Science 88(4):971-986

794 Addis DT, Patterson III WF, Dance MA, Ingram Jr. GW (2013) Implications of reef fish
795 movement from unreported artificial reed sites in the northern Gulf of Mexico. Fisheries
796 Research 147:349-358

797 Almany GR, Hamilton RJ, Bode M, Matawai M, Potuku T, Saenz-Agudelo P, Planes S,
798 Berumen ML, Rhodes KL, Thorrold SR, Russ GR, Jones GP (2013) Dispersal of grouper
799 larvae drives local resource sharing in a coral reef fishery. Current Biology 23:626-630

800 Almany GR, Planes S, THorrold SR, Berumen ML, Bode M, Saenz-Agudelo P, Bonin MC,
801 Frisch AJ, Harrison HB, Messmer V, Nanninga GB, Priest MA, Srinivasan M, Sinclair-
802 Taylor T, Williamson DH, Jones GP (2017) Larval fish dispersal in a coral-reef seascape.
803 Nature Ecology and Evolution 1:0148

804 Antoni L, Saillant E (2017) Spatial connectivity in an adult-sedentary reef fish with extended
805 pelagic larval phase. Molecular Ecology 26:4955-4965

806 Bacheler NM, Ballenger JC (2018) Decadal-scale decline of scamp (*Mycteroperca phenax*)
807 abundance along the southeast United States Atlantic coast. Fisheries Research 204:74-87

808 Bacheler NM, Shertzer KW (2015) Estimating relative abundance and species richness from
809 video surveys of reef fishes. Fishery Bulletin 113(1):15-26

810 Berenshtein I, Faillettaz R, Irisson JO, Kiflawi M, Siebeck UE, Leis JM, Paris CB (2022)
811 Evidence for a consistent use of external cues by marine fish larvae for orientation.
812 Communications Biology 5:1307

813 Berry O, England P, Fairclough D, Jackson G, Greenwood J (2012) Microsatellite DNA analysis
814 and hydrodynamic modelling reveal the extent of larval transport and gene flow between
815 management zones in an exploited marine fish (*Glaucosoma herbaicum*). Fisheries
816 Oceanography 21:4, 243-254

817 Biggs CR, Heyman WD, Farmer NA, Kobara S, Bosler DG, Robinson J, Lowerre-Barbieri SK,
818 Erisman BE (2021) The importance of spawning behavior in understanding the
819 vulnerability of exploited marine fishes in the U.S. Gulf of Mexico. PeerJ 9:e11814

820 Borden WC, Stepien CA (2006) Discordant population genetic structuring of smallmouth bass,
821 *Micropterus dolomieu* Lacepède, in Lake Erie based on mitochondrial DNA sequences
822 and nuclear DNA microsatellites. Journal of Great Lakes Research 32:242-257

823 Botsford LW, White JW, Coffroth MA, Paris CB, Planes S, Shearer TL, Thorrols SR, Jones GP
824 (2009) Connectivity and resilience of coral reef metapopulations in marine protected
825 areas: matchin empirical efforts to predictive needs. Coral Reefs 28:327-337

826 Bottesch M, Gerlach G, Halback M, Bally A, Kingsfod MJ, Mouritsen H (2016) A magnetic
827 compass that might help coral reef fish larvae return to their natal reef. Current Biology
828 26:R1247-R1271

829 Bonanomi S, Therkildsen NO, Retzel A, Hedholm RB, Pederson MW, Meldrup D, Pampoulie C,
830 Hemmer-Hansen J, Gronkjaer P, Nielsen EE (2016) Historical DNA documents long-
831 distance natal homing in marine fish. Molecular Ecology 25(12):2727-2734

832 Bullock LH, Smith GB (1991) Memoirs of the hourglass cruises: seabasses (Pisces: Serranidae).
833 Florida Marine Research Institute, Department of Natural Resources, St. Petersburg,
834 Florida

835 Buston PM, Jones GP, Planes S, Thorrold SR (2012) – Probability of successful larval dispersal
836 declines fivefold over 1 km in a coral reef fish. Proceedings of the Royal Society B
837 279:1883-1888

838 Campbell MD, Pollack AG, Gledhill CT, Switzer TS, DeVries DA (2015) Comparison of
839 relative abundance indices calculated from two methods of generating video count data.
840 Fisheries Research 170:125-133

841 Campbell RA, Gales NJ, Lento GM, Baker CS (2008) Islands in the sea: extreme female natal
842 site fidelity in the Australian sea lion, *Neophoca cinerea*. Biology Letters 4:139-142

843 Carr MH, Robinson SP, Wahle C, Davis G, Kroll S, Murray S, Schumacker EJ, Williams M
844 (2017) The central importance of ecological spatial connectivity to effective coastal
845 marine protected areas and to meeting the challenges of climate change in the marine
846 environment. Aquatic Conservation: Marine and Freshwater Ecosystems 27:6-29

847 Chassignet EP, Hurlburt HE, Smedstad OM, Halliwell GR, Hogan PJ, Wallcraft AJ, Baraille R,
848 Bleck R (2007) The HYCOM (Hybrid Coordinate Ocean Model) data assimilative
849 system. Journal of Marine Systems 65:60-83

850 Coleman FC, Scanlon KM, Koenig C (2011) Groupers on the edge: shelf edge spawning habitat
851 in and around marine reserves of the northeastern Gulf of Mexico. The Professional
852 Geographer 63(4):1-19

853 Colin PL, Koenig CC, Laroche WA (1996) Development from egg to juvenile of the red grouper
854 (*Epinephelus morio*) (Picses: Serranidae) in the laboratory. In: Arreguín-Sánchez F,
855 Munro JL, Balgos MC, Pauly D (eds) Biology, fisheries and culture of tropical groupers
856 and snappers. International Center for living Aquatic Resources Management. Manila,
857 Philippines

858 Coleman F, Scanlon KM, Koenig CC (2011) Groupers on the edge: shelf edge spawning habitat
859 in and around marine reserves of the northeastern Gulf of Mexico. The Professional
860 Geographer 63(4):456-474

861 Cowen RK, Paris CB, Fortuna JL, Olson DB (2003) The role of long distance dispersal versus
862 local retention in replenishing marine populations. Gulf and Caribbean Research
863 14(2):129-137

864 Cowen RK, Paris CB, Srinivasan A (2006) Scaling connectivity in marine populations, Science
865 311:522-527

866 Cresci A, Paris CB, Foretich MA, Durif SM, Shema SD, O'Brien CJE, Vikebø, Skiftesvik AB,
867 Browman HI (2019) Atlantic haddock (*Melanogrammus aelefinus*) larvae have a
868 magnetic compass that guides their orientation. iScience 19:1173-1178

869 D'Aloia CC, Bogdanowicz SM, Francis RK, Majoris JE, Harrison RG, Buston PM (2015)
870 Patterns, causes, and consequences of marine larval dispersal. PNAS 112(45):13940-
871 13945

872 D'Aloia CC, Bogdanowicz SM, Andrés JA, Buston PM (2022) Population assignment tests
873 uncover rare long-distance marine larval dispersal events. Ecology 103(1):e03559

874 Di Stefano M, Legrand T, Di Franco A, Nerini D, Rossi V (2023) Insights into the spatio-
875 temporal variability of spawning in a territorial coastal fish by combining observations,
876 modeling and literature review. Fisheries Oceanography 32:70-90

877 Druon JN, Fiorentino F, Murenu M, Knittweis L, Colloca F, Osio C, Mérigot B, Garofalo G,
878 Mannini A, Jadaud A, Sbrana M, Scarcella G, Tserpes G, Peristeraki P, Carlucci R,
879 Heikkonen J (2015) Modelling of European hake nurseries in the Mediterranean Sea: An
880 ecological niche approach. Progress in Oceanography 130:188-204

881 Dubois M, Rossi V, Ser-Giacomi E, Arnaud-Haond S, López C, Hernández-García (2016)
882 Linking basin-scale connectivity, oceanography and population dynamics for the
883 conservation and management of marine ecosystems. Global Ecology and Biogeography
884 25:503-515

885 Erisman B, Heyman W, Kobara S, Ezer T, Pittman S, Aburto-Oropeza O, Nemeth RS (2017)
886 Fish spawning aggregations: where well-placed management actions can yield big
887 benefits for fisheries and conservation. Fish and Fisheries 18:128-144

888 Faillettaz R, Blandin A, Paris SB, Koubbi P, Irisson JO (2015) Sun-compass orientation in
889 mediterranean fish larvae. PLoS ONE 10(8):e0135213

890 Faillettaz R, Paris CB, Irisson J (2018) Larval fish swimming behavior alters dispersal patterns
891 from marine protected areas in the north-western Mediterranean Sea. Frontiers in Marine
892 Science 5:97

Farmer NA, Heyman WD, Karnauskas M, Kobara S, Smart TL, Ballenger JC, Reichert MJM, Wyanski DM, Tishler MS, Lindeman KC, Lowerre-Barbieri SK, Switzer TS, Solomon JJ, McCain K, Marhefka M, Sedberry GR (2017) Timing and locations of reef fish spawning off the southeastern United States. PLoS ONE 12(3):e0172968

Fitzhugh GR, Koenig CC, Coleman FC, Grimes CB, Sturges III WS (2005) Spatial and temporal patterns in fertilization and settlement of young gag (*Mycteroperca microlepis*) along the West Florida Shelf. Bulletin of Marine Science 77(3):377-396

Gabriele G, Atema J, Kingsford MJ, Black KP, Miller-Sims V (2007) Smelling home can prevent dispersal of reef fish larvae. PNAS 104(3):858-863

Gardner MJ, Chaplin JA, Potter IC, Fairclough DV (2015) Pelagic early life stages promote connectivity in the desmersal labrid *Choerodon rubescens*. Journal of Experimental Marine Biology and Ecology 472:142-150

Gilmore RG, Jones RS (1992) Color variation and associated behavior in the Epinepheline groupers, *Mycteroperca microlepis* (Goode and Bean) and *M. phenax* Jordan and Swain. Bulletin of Marine Science 51(1):83-103

Grüss A, Biggs CR, Heyman WD, Erisman B (2018) Prioritizing monitoring and conservation efforts for fish spawning aggregations in the U.S. Gulf of Mexico. Scientific Reports 8:8473

Harris PJ, Wyanski DM, Byron White D, Moore JL (2002) Age, growth, and reproduction of scamp, *Mycteroperca phenax*, in the southwestern north Atlantic, 1979-1997. Bulletin of Marine Science 70(1):113-132

Hernández CM, Paris CB, Vaz AC, Jones BT, Kellner JB, Richardson DE, Sponaugle S, Cowen RK, Llopiz JK (2023) Diverse patterns of larval coral reef fish vertical distribution and consequences for dispersal and connectivity. Coral Reefs 42:453-465

Hetland RD, Hsueh Y (1999) A loop current-induced jet along the edge of the West Florida Shelf. Geophysical Research Letters 26(15):2239-2242

Heyman WD, Grüss A, Biggs CR, Kobara S, Farmer NA, Karnauskas M, Lowerre-Barbieri S, Erisman B (2019) Cooperative monitoring, assessment, and management of fish spawning aggregations and associated fisheries in the U.S. Gulf of Mexico. Marine Policy 109:103689

Hidalgo M, Rossi V, Monroy P, Ser-Giacomi E, Hernández-García E, Guijarro B, Massutí E, Alemany F, Jadaud A, Luis Perez J, Reglero P (2019) Accounting for ocean connectivity and hydroclimate in fish recruitment fluctuations within transboundary metapopulations. Ecological Applications 29(5):e01913

Hyun KH, He R (2010) Coastal upwelling in the South Atlantic Bight: a revisit of the 2003 cold event using long term observations and model hindcast solutions. Journal of Marine Systems 83:1-13

930 Jones GP, Milicich MJ, Emslie MJ, Lunow C (1999) Self-recruitment in a coral reef fish
931 population. Nature 402:802-804

932 Jones GP, Planes S, Thorrold SR (2005) Coral reef fish settle close to home. Current Biology
933 15:1314-1318

934 Karnauskas M, Shertzer KW, Paris CB, Farmer NA, Switzer TS, Lowerre-Barbieri SK, Kellison
935 GT, He Ruoying, Vaz AC (2022) Source-sink recruitment of red snapper: connectivity
936 between the Gulf of Mexico and Atlantic Ocean. Fisheries Oceanography 31(6):571-586

937 Keener P, Johnson GD, Stender BW, Brothers EB, Beatty HR (1988) Ingress of postlarval gag,
938 *Mycteroperca microlepis* (Pisces: Serranidae), through a South Carolina barrier island
939 inlet. Bulletin of Marine Science 42(3):376-396

940 Keller J, Herbig J, Acosta A (2020) Fisheries-independent data for scamp (*Mycteroperca*
941 *phenax*) from reef-fish visual surveys in the Florida Keys and Dry Tortugas, 1999-2018.
942 SEDAR68-DW-06. SEDAR, North Charleston, SC, 25 pp

943 Kingsford MJ, Leis JM, Shanks A, Lindeman KC, Morgan SG, Pineda J (2002) Sensory
944 environments, larval abilities and local self-recruitment. Bulletin of Marine Science
945 70(1):309-340

946 Klein JD, Asbury TA, da Silva C, Hull KL, Dicken ML, Gennari E, Maduna SN, Bester-van der
947 Merwe AE (2020) Site fidelity and shallow genetic structure in the common smooth-
948 hound shark *Mustelus mustelus* confirmed by tag-recapture and genetic data. Journal of
949 Fish Biology 100:134-149

950 Le Corre N, Pepin P, Han G, Ma Z, Snelgrove PVR (2018) Assessing connectivity patterns
951 among management units of the Newfoundland and Labrador shrimp population.
952 Fisheries Oceanography 28(2):183-202

953 Le Corre N, Pepin P, Burmeister A, Walkusz W, Skanes K, Wang Z, Brickman D, Snelgrove
954 PVR (2020) Larval connectivity of northern shrimp (*Pandalus borealis*) in the Northwest
955 Atlantic. Canadian Journal of Fisheries and Aquatic Science 77(8):1332-1347

956 Le Hénaff M, Kourafalou VH (2016) Mississippi water reaching South Florida reefs under no
957 flood conditions: synthesis of observing and modeling system findings. Ocean Dynamics
958 66:435-459

959 Legrand T, Chenuil A, Ser-Giacomi E, Arnaud-Haond S, Bierne N, Rossi V (2022) Spatial
960 coalescent connectivity through multi-generational dispersal modeling predicts gene flow
961 across marine phyla. Nature Communications 13:5861

962 Lellouche J, Greiner E, Le Galloudec O, Garric G, Reginier C, Drévillon M, Benkiran M, Testut
963 C, Bourdallé-Badie R, Gasparin F, Hernandez O, Levier B, Drillet Y, Remy E, Le Traon
964 P (2018) Recent updates to the Copernicus Marine Service global ocean monitoring and
965 forecasting real-time 1/12° high-resolution system. Ocean Science 14:1093-1126

966 Lellouche J, Greiner E, Bourdallé-Badie R, Garric G, Melet A, Drévillon M, Bricaud C, Hamon
967 M, Le Galloudec O, Reginier C, Candela T, Testut C, Gasparin F, Ruggieo G, Benkiran
968 M, Drillet Y, Le Traon P (2021) The Copernicus global 1/12° oceanic and sea ice
969 GLORYS12 reanalysis. Frontiers in Earth Science 9:698876

970 Lindeman KC, Pugliese R, Welch GT, Ault JS (2000) Developmental patterns within a
971 multispecies reef fishery: management applications for essential fish habitats and
972 protected areas. Bulletin of Marine Science 66(3):929-956

973 Liu Y, Weisberg RH, Vignudelli S, Mitchum GT (2016) Patterns of the loop current system and
974 regions of sea surface height variability in the eastern Gulf of Mexico revealed by the
975 self-organizing maps. Journal of Geophysical Research: Oceans 121:2347-2366

976 Lombardi-Carlson LA, Cook M, Lyon H, Barnett B, Bullock L (2012) A description of age,
977 growth, and reproductive life-history traits of scamps from the northern Gulf of Mexico.
978 Marine and Coastal Fisheries 4(1):129-144

979 Lowe WH, Allendorf FW (2010) What can genetics tell us about population connectivity?
980 Molecular Ecology 19:3038-3051

981 Lowther AD, Harcourt RG, Goldsworthy SD, Stow A (2012) Population structure of adult
982 female Australian sea lions is driven by fine-scale foraging site fidelity. Animal
983 Behaviour 83(3):691-701

984 Marra G, Wood SN (2011) Practical variable selection for generalized additive models.
985 Computational Statistics and Data Analysis 55(7):2372-2387

986 Meylan AB, Bowen BW, Avise JC (1990) A genetic test of the natal homing versus social
987 facilitation models for green turtle migration. Science 248(4956):724-727

988 Milot E, Weimerskirch H, Bernatchez L (2008) The seabird paradox: dispersal, genetic structure
989 and population dynamics in a highly mobile, but philopatric albatross species. Molecular
990 Ecology 17:1658-1673

991 Montgomery JC, Tolimieri N, Haine OS (2001) Active habitat selection by pre-settlement reef
992 fishes. Fish and Fisheries 2:261-277

993 National Academies of Sciences, Gulf Research Program and Committee on Advancing
994 Understanding of Gulf of Mexico Loop Current Dynamics (2018) Understanding and
995 predicting the Gulf of Mexico loop current: critical gaps and recommendations. National
996 Academies Press.

997 NOAA National Geophysical Data Center, U.S. Coastal Relief Model Volumes 2, 3, 4, 5.
998 https://www.ncei/noaa/gov/products/coastal-relief-model

999 Okubo A (1971) Oceanic diffusion diagrams. Deep-Sea Research 18:789-802

1000 Palumbi SR (2003) Population genetics, demographic connectivity, and the design of marine
1001 reserves. Ecological Applications 13(1):S146-S158

1002 Paris CB, Helgers J, van Sebille E, Srinivasan A (2013) Connectivity Modeling System: a
1003 probabilistic modeling tool for the multi-scale tracking of biotic and abiotic variability in
1004 the ocean. Environmental Modelling and Software 42:47-54

1005 Pearce JM, Blums P, Lindberg MS (2008) Site fidelity is an inconsistent determinant of
1006 population structure in the hooded merganser (*Lophodytes cucllatus*): evidence from
1007 genetic, mark-recapture, and comparative data. The Auk 125(3):711-722

1008 Poisot T (2011) The digitize package: extracting numerical data from scatterplots. The R Journal
1009 3.1:25-26

1010 Punt AE, Butterworth DS, de Moor CL, De Oliveira JAA, Haddon M (2016) Management
1011 strategy evaluation: best practices. Fish and Fisheries 17(2):303-334

1012 R Core Team (2023) R: a language and environment for statistical computing. R Foundation for
1013 Statistical Computing, Vienna, Austria, https://www.R-project.org/

1014 Roberts DE, Schlieder RA (1983) Induced sex inversion, maturation, spawning and embryogeny
1015 of the protogynous grouper, *Mycteroperca microlepis*. Journal of the World Mariculture
1016 Society 14:639-649

1017 Rooker JR, Secor DH, DeMetrio G, Schloesser R, Block BA, Neilson JD (2008) Natal homing
1018 and connectivity in Atlantic bluefin tuna populations. Science 322(5902):742-744

1019 South Atlantic Fishery Management Council MPA Expert Work Group (2013) Report of the
1020 second meeting of the MPA expert work group. Crown Plaza Hotel, North Charleston,
1021 SC, 45 pp

1022 Schobernd CM, Sedberry GR (2009) Shelf-edge and upper-slope reef fish assemblages in the
1023 south Atlantic bight: habitat characteristics, spatial variation, and reproductive behavior.
1024 Bulletin of Marine Science 84(1):67-92

1025 Schobernd ZH, Bacheler NM, Conn PB (2014) Examining the utility of alternative video
1026 monitoring metrics for indexing reef fish abundance. Canadian Journal of Fisheries and
1027 Aquatic Sciences 71(3):464-471

1028 SEDAR (2020) Gulf of Mexico and Atlantic scamp stock ID process final report. SEDAR68-
1029 SID-05, SEDAR, North Charleston, SC, 42 pp

1030 SEDAR (2022a) SEDAR 68OA – Gulf of Mexico scamp grouper final stock assessment report.
1031 SEDAR, North Charleston, SC, 202 pp

1032 SEDAR (2022b) SEDAR 68 south Atlantic scamp stock assessment report. SEDAR, North
1033 Charleston, SC, 162 pp

1034 Selkoe KA, D'Aloia CC, Crandall ED, Iacchei M, Liggins L, Puritz JB, von der Heyden S,
1035 Toonen RJ (2016) A decade of seascape genetics: contributions to basic and applied
1036 marine connectivity. Marine Ecology Progress Series 554:1-19

1037 Smith CL (1971) A revision of the American groupers: *Epinephelus* and allied genera. Bulletin
1038 of the American Museum of Natural History 146(2)69-241

1039 Swearer SE, Treml EA, Shima JS (2019) A review of biophysical models of marine larval
1040 dispersal. Oceanography and Marine Biology: An Annual Review 57:325-356

1041 Teodósio MA, Paris CB, Wolanski E, Morais P (2016) Biophysical processes leading to the
1042 ingress of temperate fish larvae into estuarine nursery areas: a review. Estuarine, Coastal
1043 and Shelf Science 183(A):187-202

1044

1045 Thompson KA, Switzer TS, Christman MC, Keenan SF, Gardner C, Overly KE, Campbell M
1046 (2020) Indices of abundance for scamp (*Mycteroperca phenax*) using combined data
1047 from three independent video surveys. SEDAR68-DW-07, SEDAR, North Charleston,
1048 SC, 19 pp

1049 Thorrold SR, Latkoczy C, Swart PK, Jones CM (2001) Natal homing in a marine fish
1050 metapopulation. Science 291:297-299

1051 van Herwerden L, Aspden WJ, Newman SJ, Pegg GG, Briskey L, Sinclair W (2009) A
1052 comparison of the population genetics of *Lethrinus miniatus* and *Lutjanus sebae* from the
1053 east and west coasts of Australia: evidence for panmixia and isolation. Fisheries Research
1054 100:148-155

1055 Vaz AC, Karnauskas M, Paris CB, Doerr JC, Hill RL, Horn C, Miller MH, Neuman M,
1056 McCarthy KJ, Farmer NA (2022) Exploitation drives changes in the population
1057 connectivity of queen conch (*Aliger gigas*). Frontiers in Marine Science 9:841027

1058 Vaz AC, Karnauskas M, Smith M, Denson LS, Paris CB, Le Hénaff M, Siegfried K (2023) Red
1059 Snapper connectivity in the Gulf of Mexico. Marine and Coastal Fisheries: Dynamics,
1060 Management, and Ecosystem Science 15:e10275

1061 Weersing K, Toonen RJ (2009) Population genetics, larval dispersal, and connectivity in marine
1062 systems. Marine Ecology Progress Series 393:1-12

1063 Weisberg RH and Liu Y (2017) On the Loop Current penetration into the Gulf of Mexico.
1064 Journal of Geophysical Research: Oceans 122:9679-9694

1065 Whitney NM, Robbins WD, Schultz JK, Bowen BW, Holland KN (2012) Oceanic dispersal in a
1066 sedentary reef shark (*Triaenodon* obesus): genetic evidence for extensive connectivity
1067 without a pelagic larval stage. Journal of Biogeography 39: 1144-1156

1068 Wilson RR, Burns KM (1996) Potential survival of released groupers caught deeper than 40 m
1069 based on shipboard and in-situ observations, and tag-recapture data. Bulletin of Marine
1070 Science 58(1):234-247

1071 Wood SN (2011) Fast stable restricted maximum likelihood and marginal likelihood estimation
1072 of semiparametric generalized linear models. Journal of the Royal Statistical Society B
1073 73(1):3-36

1074 Xue Z, Zambon J, Yao Z, Liu Y, He R (2015) An integrated ocean circulation, wave,
1075 atmosphere, and marine ecosystem prediction system for the South Atlantic Bight and
1076 Gulf of Mexico. Journal of Operational Oceanography 8(1):80-91

1077 Young EF, Belchier M, Hauser L, Horsburgh GJ, Meredith MP, Murphy EJ, Pascoal S, Rock J,
1078 Tysklind N, Carvalho GR (2015) Oceanography and life history predict contrasting
1079 genetic population structure in two Antarctic fish species. Evolutionary Applications
1080 8(5):486-509

1081 Zatcoff MS, Ball AO, Sedberry GR (2004) Population genetic analysis of red grouper,
1082 *Epinephelus morio*, and scamp, *Mycteroperca phenax*, from the southeastern U.S.
1083 Atlantic and Gulf of Mexico. Marine Biology 144:769-777

1084 Zeng X, Adams A, Roffer M, He R (2018) Potential connectivity among spatially distinct
1085 management zones for Bonefish (*Albua vulpes*) via larval dispersal. Environmental
1086 Biology of Fishes 102:233-252

7. TABLES

Table 1: Simulation configurations. Eight larval dispersal simulations, including a base simulation and seven sensitivity simulations that investigate variation due to uncertainty in the ocean velocity estimates and scamp larval biology. OVM (ontogenetic vertical migration) indicates whether the simulation includes an ontogenetic shift in the vertical distribution of simulated larvae. H indicates simulations included in the hydrodynamic ensemble and B indicates simulations included in the biological ensemble. PLD = pelagic larval duration, HYCOM = Hybrid Coordinate Ocean Model, GOM = Gulf of Mexico, GOFS = Global Ocean Forecasting System, HiRes = high resolution, IAS = Inter-American Seas, SABGOM = South Atlantic Bight and Gulf of Mexico.

Simulation	Hydrodynamic Product	Competency Period (PLD)	OVM	Settlement Criteria	Ensemble
Base	HYCOM GOM + GOFS	33-52 days	N	30	H,B
GOM HiRes	HYCOM GOM HiRes + GOFS	33-52 days	No	30 m	H
IA	HYCOM IAS	33-52 days	N	30	H
Mercator	Mercator	33-52 days	No	30 m	H
SABGOM	SABGOM	33-52 days	N	30	H
PLD 57	HYCOM GOM + GOFS	33-57 days	No	30 m	B
OVM	HYCOM GOM + GOFS	33-52 days	Yes	30	B
45m	HYCOM GOM + GOFS	33-52 days	No	45 m	B

Table 2: Vertical distribution of simulated larvae. The percentage of simulated larvae in each depth bin for each of two vertical distribution assumptions. Most simulations assumed a single vertical distribution throughout the entire pelagic larval duration. One sensitivity simulation, however, assumed an ontogenetic shift in the vertical distribution of larvae. CMS uses these distributions, which we calculated by analyzing empirical data (Appendix 4), to specify the vertical distribution of simulated larvae in each timestep. PLD = pelagic larval duration.

Depth Bin	No Ontogenetic Shift	Ontogenetic Shift	
	Entire PLD	Pre-flexion	Post-flexion
0-20 meters	6	6	4
20 to 40 meters	30	28	48
40 to 60 meters	1	8	1
60 to 100 meters	0	0	0

Table 3: Hydrodynamic product specifications. Our simulations used ocean velocity fields from six different hydrodynamic products with varying specifications. See Table 1 for how these fields were applied across the simulations – note that the GOFS fields were only used as a nest for other products that did not cover the entire region of interest. Appendix 6 (Supplemental Materials) provides more details for each hydrodynamic product. HYCOM = Hybrid Coordinate Ocean Model, GOM = Gulf of Mexico, HiRes = high resolution, IAS = Inter-American Seas, SABGOM = South Atlantic Bight and Gulf of Mexico, GOFS = Global Ocean Forecasting System.

Hydrodynamic Product	Years	Vert. Resolution (top 100m)	Horiz. Resolution	Type of Product	CMS Diffusivity Coefficient
HYCOM GOM	2012, 2013, 2015-2018	20 layers	1/25° (ca. 4km)	Hindcast	15 m^2/s
HYCOM GOM HiRes	2011-2017	11 layers	1/50° (ca. 2km)	Hindcast	12 m^2/s
HYCOM IAS	2010	7 layers	1/32° (ca. 3.5km)	Reanalysis	15 m^2/s
MERCATOR	2013-2017	22 layers	1/12° (ca. 8km)	Reanalysis	20 m^2/s
SABGOM	2004-2010	20 layers	1/25° (ca. 4km)	Hindcast	20 m^2/s
GOFS Expt. 3.0	2011-2014	7 layers	1/12° (ca. 8km)	Hindcast	20 m^2/s
GOFS Expt. 3.1	2015-2018	20 layers			

Table 4: All proportions by simulation. We calculated several proportions to describe the connectivity dynamics between the U.S. Gulf of Mexico (GOM) and Atlantic (ATL). Columns 2-4 describe what percentage of recruits to various portions of the Atlantic came from spawning in the Gulf of Mexico. Columns 5 and 6 describe what percentage of simulated larvae from each region successfully settled anywhere. The last column describes what percentage of successful larvae spawned from Gulf of Mexico spawning areas settled in the Atlantic. H indicates simulations included in the hydrodynamic ensemble and B indicates simulations included in the biological ensemble. GOM = Gulf of Mexico, HiRes = high resolution, IAS = Inter-American Seas, SABGOM = South Atlantic Bight and Gulf of Mexico, PLD = pelagic larval duration, OVM = ontogenetic vertical migration.

Simulation (Ensemble)	% ATL recruits from GOM	% ATL recruits (N of 25.75) from GOM	% ATL recruits (N of 28.5) from GOM	% ATL Spawn Settled	% GOM Spawn Settled	% GOM to ATL
Base (H, B)	34	19	10	25	26	7
GOM HiRes (H)	56	21	9	39	26	11
IAS (H)	25	9	5	32	27	4
Mercator (H)	55	11	4	31	23	11
SABGOM (H)	19	3	2	27	20	2
PLD 57 (B)	36	22	12	27	27	7
OVM (B)	29	18	10	19	32	9
45m (B)	43	34	28	41	30	7

Table 5: Percentage of recruits to the U.S. Atlantic that came from Gulf of Mexico spawning locations. H indicates simulations included in the hydrodynamic ensemble and B indicates simulations included in the biological ensemble. GOM = Gulf of Mexico, HiRes = high resolution, IAS = Inter-American Seas, SABGOM = South Atlantic Bight and Gulf of Mexico, PLD = pelagic larval duration, OVM = ontogenetic vertical migration.

Year	Base (H,B)	GOM HiRes (H)	IAS (H)	Mercator (H)	SABGOM (H)	PLD 57 (B)	OVM (B)	45m (B)
2004	-	-	-	-	35	-	-	-
2005	-	-	-	-	16	-	-	-
2006	-	-	-	-	21	-	-	-
2007	-	-	-	-	26	-	-	-
2008	-	-	-	-	20	-	-	-
2009	-	-	-	-	12	-	-	-
2010	-	-	25	-	12	-	-	-
2011	-	61	-	-	-	-	-	-
2012	-	29	-	-	-	-	-	-
2013	28	65	-	76	-	30	24	-
2014	-	51	-	26	-	-	-	-
2015	25	59	-	31	-	27	23	31
2016	45	47	-	57	-	49	38	55
2017	37	74	-	49	-	38	34	44
2018	25	-	-	-	-	28	18	30
All	34	56	25	55	19	36	29	43

8. FIGURES

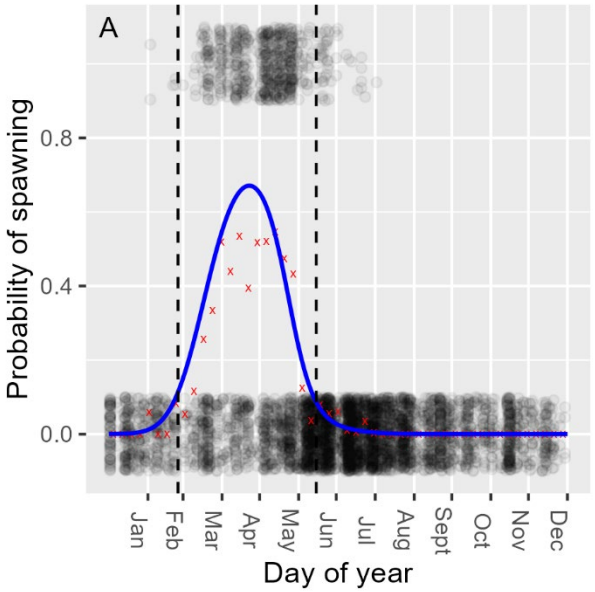

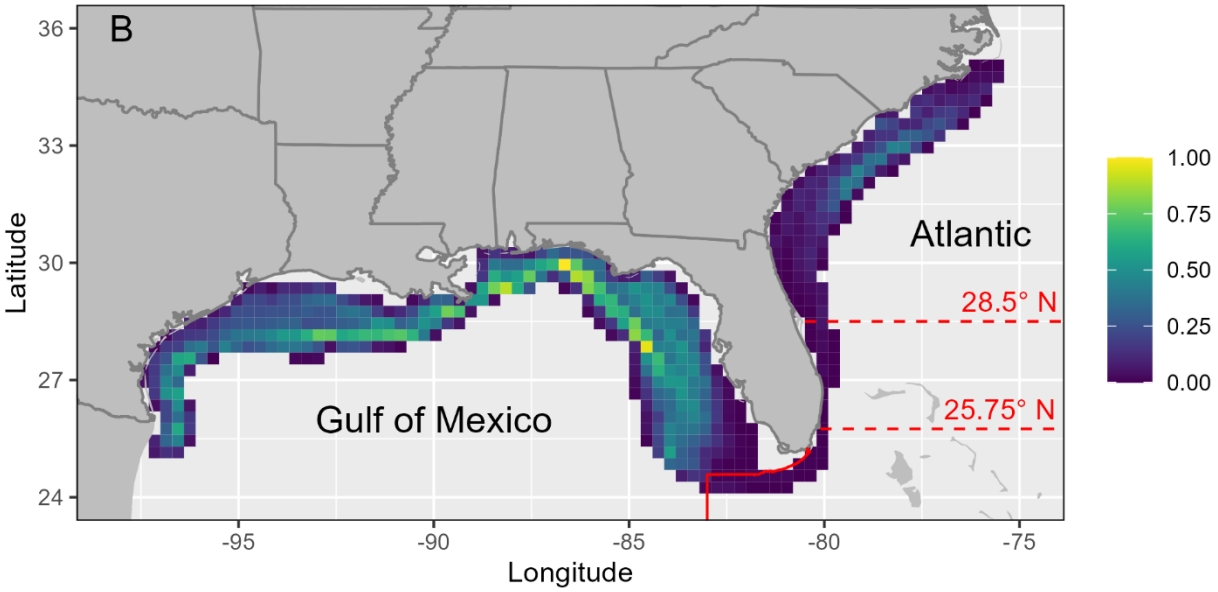

Figure 1: The seasonal (A) and spatial (B) distribution of scamp spawning, which is proportional to the amount of simulated spawning. A) GAM predicts that scamp spawning peaks in late April. The dashed lines show the spawning season during which we simulated spawning. The number of larvae simulated on any given day was proportional to the predicted probability of spawning (blue line). The jittered black points show the catch date of all histological samples. Points along the top are females within 24 hours of spawning and points along the bottom are from non-spawning females or males. The red x's show the proportion of samples that came from spawning females in weekly bins. B) A map showing the predicted

spatial distribution of scamp spawning with values proportional to the maximum. Yellow indicates high estimated spawning and purple indicates low estimated spawning. We used this distribution to scale the amount of spawning simulated from each grid location. The solid red line shows the boundary between the U.S. Gulf of Mexico and South Atlantic management units, and the dashed red lines delineate sub-regions within the Atlantic.

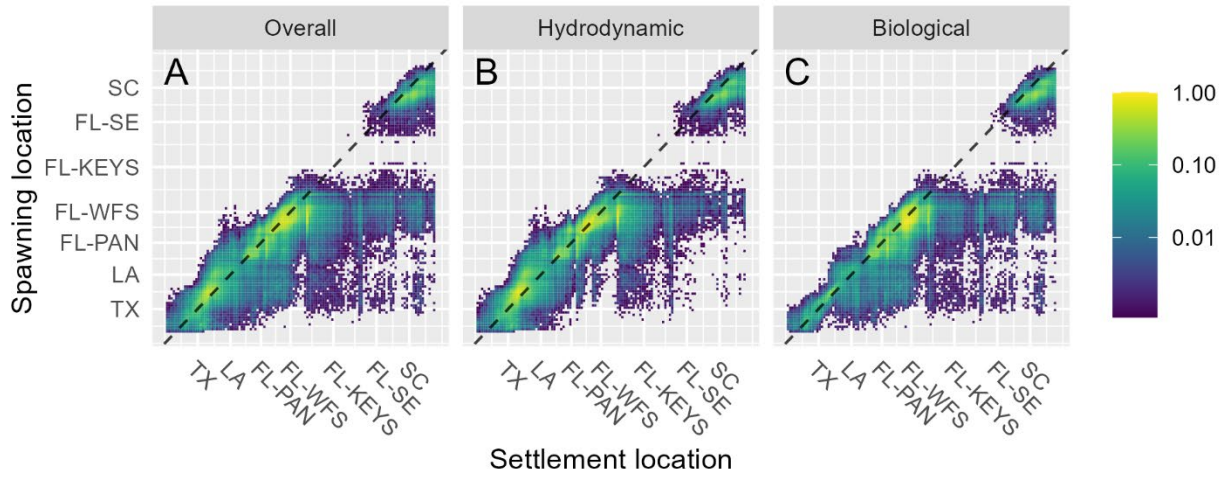

Figure 2: Connectivity matrices showing the dispersal dynamics of successful simulated scamp larvae summarized over the overall (A), hydrodynamic (B), and biological (C) ensembles. The vertical axis represents the spawning location, and the horizontal axis represents shows the settlement location of successful virtual larvae. The values (on a log scale) are proportional to the maximum across all panels with yellow indicating high estimated connectivity and purple indicating low estimated connectivity. The black dotted line represents the axis of local retention (i.e., settlement location = spawning location, Botsford et al. 2009). TX = Texas, LA = Louisiana, FL-Pan = the Florida Panhandle, FL-WFS = the West Florida Shelf, FL-Keys = the Florida Keys, FL-SE = the Atlantic coast of Florida, SC = South Carolina. These geographic sub-regions follow the U.S. coastline from west to east and are identified in supplemental figure S7. Supplemental figure S12 shows a similar connectivity matrix for each individual simulation.

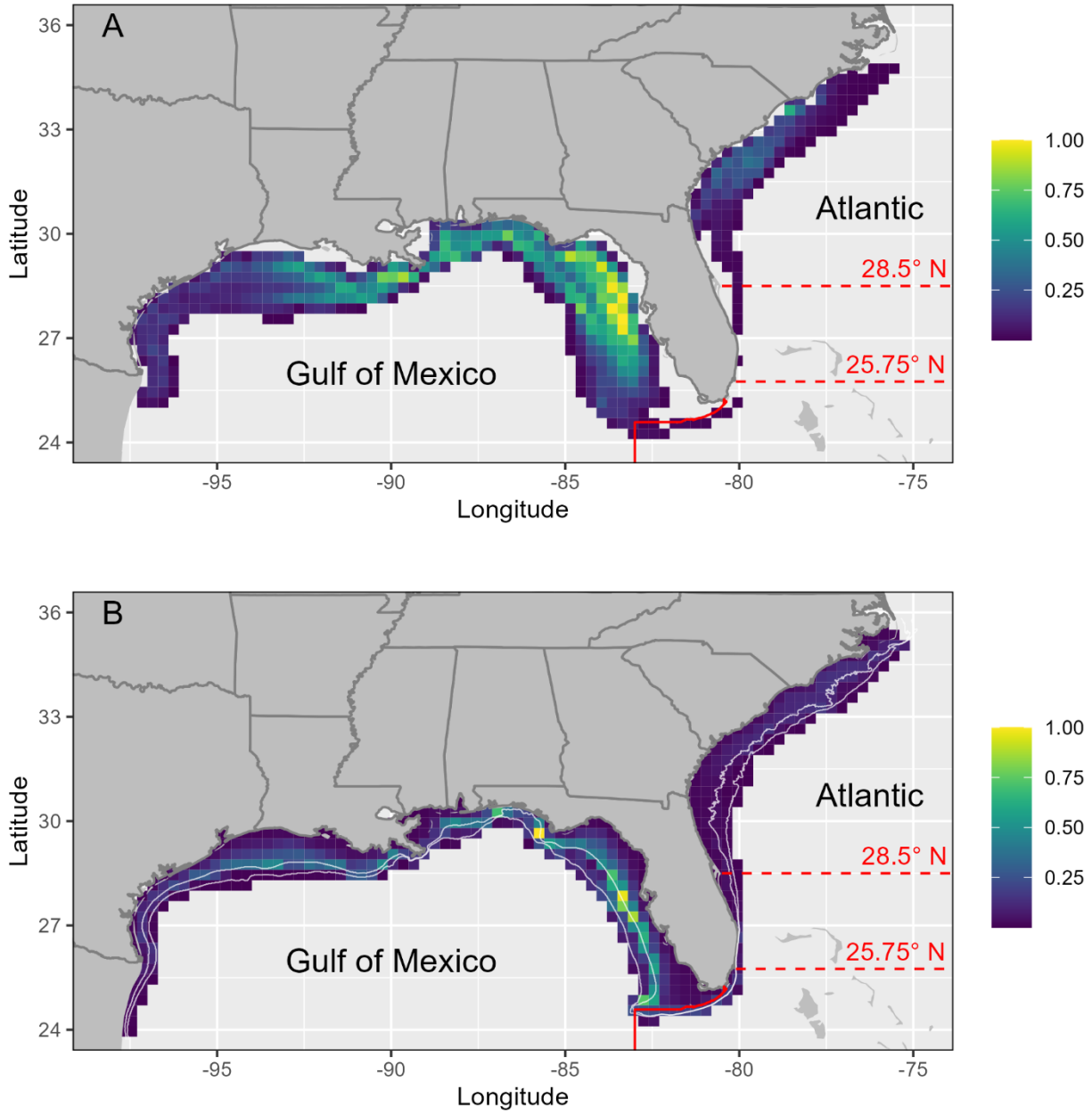

Figure 3: Spatial distribution of spawning (A) and settlement (B) locations of successful simulated scamp larvae. Values are proportional to the maximum, with yellow indicating an area where many successful virtual were spawned or settled, and purple indicating an area where few successful larvae were spawned or settled. These maps show the results of the overall ensemble that pooled all simulations. Supplemental figures (S13 and S14) show the hydrodynamic and biological ensembles individually. The solid red line shows the boundary between the U.S. Gulf of Mexico and Atlantic management units, and the dashed red lines delineate sub-regions within the Atlantic. The white lines (B) represent two alternative assumptions for settlement habitat. For the base simulation, settlement habitat included any

location between the coastline and the 30-meter isobath. For one of the sensitivity analyses settlement habitat was extended to the 45-meter isobath.

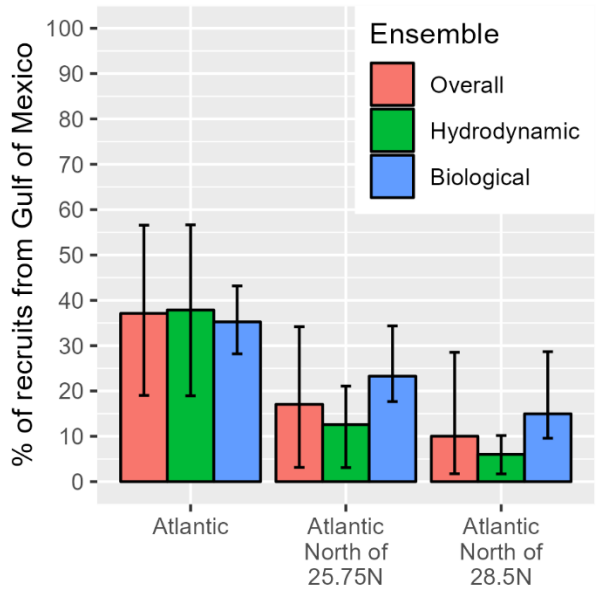

Figure 4: The proportion of recruits to the Atlantic that came from the Gulf of Mexico. We resampled each simulation 1000 times and calculated the proportion for each resample. Then, we pooled the resampled proportions from the simulations in an ensemble and calculated the ensemble mean (bars) and standard deviation (error bars). This captures the uncertainty within each simulation as well as across the simulations in an ensemble.

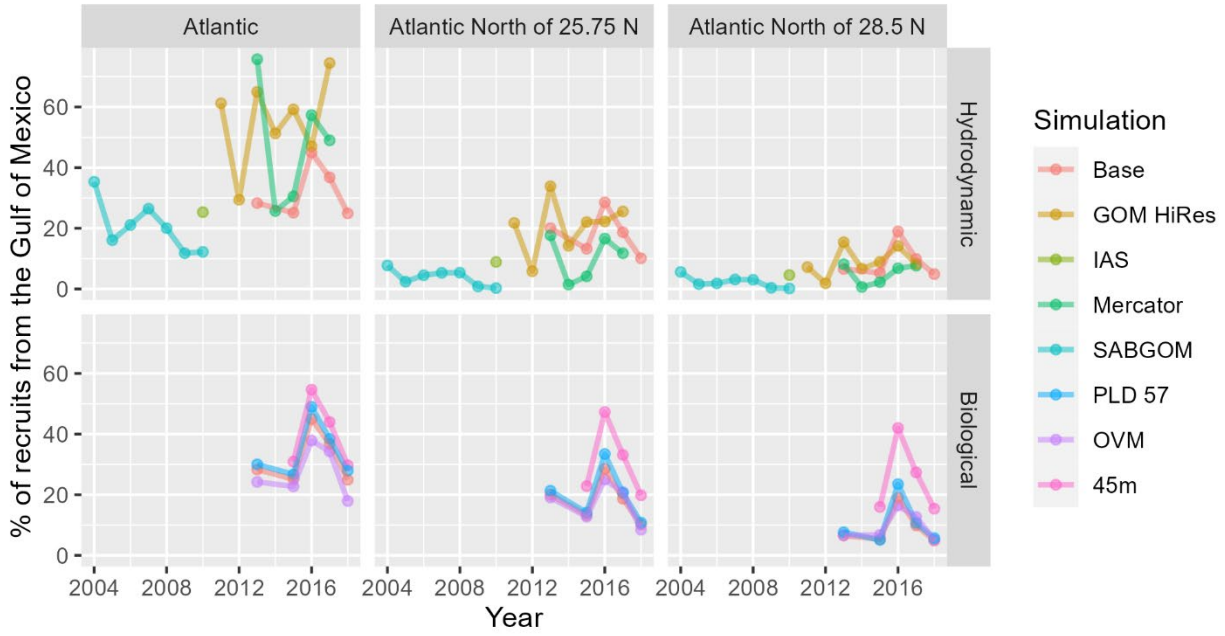

Figure 5: The proportion of recruits to the Atlantic that come from the Gulf of Mexico by simulation and year. Each simulation is colored differently, with simulations in the hydrodynamic ensemble simulations along the top row and simulations in the biological ensemble along the bottom row. Note that the "Base" simulation is in both ensembles. The lines connecting data points do not represent a regression or trend and are only included to highlight the year-to-year changes within a simulation. Each column shows the proportion based on recruitment to a different portion of the Atlantic.

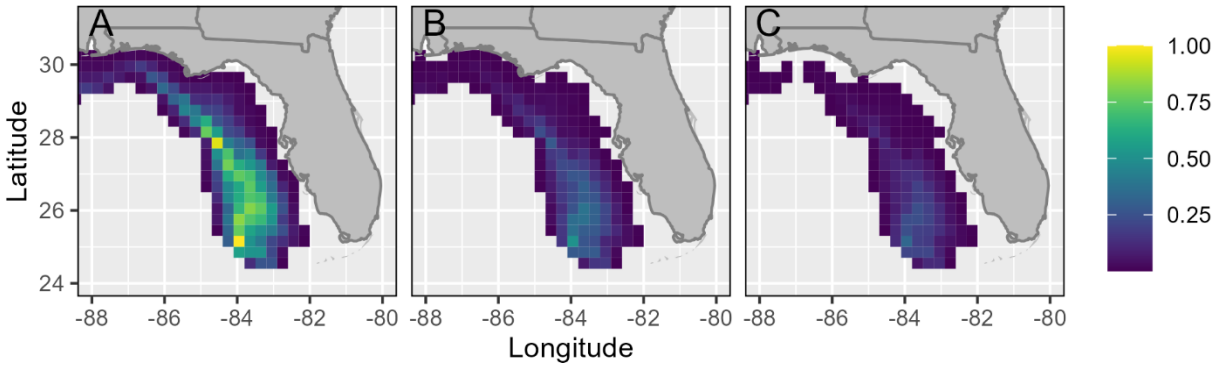

Figure 6: Distribution of the spawning locations for Atlantic recruits that came from the Gulf of Mexico. Values are proportional to the maximum across all panels. Yellow indicates spawning areas that produced a high number of Gulf to Atlantic recruits and purple indicates spawning areas that produced a low number of Gulf to Atlantic recruits. Each panel represents the spawning locations for recruits that started in the Gulf of Mexico and ended in a different portion of the Atlantic: the entire Atlantic (A), the Atlantic north of 25.75° N (B), and the Atlantic north of 28.5° N (C). These maps show the results from the overall ensemble that pools all simulations.